Detecting Anthropogenic CO_2 Changes in the Interior Atlantic Ocean between 1989-2005

Rik Wanninkhof[1]
Scott C. Doney[2]
John L. Bullister[3]
Naomi M. Levine[2*]
Mark Warner[4]
Nicolas Gruber[5]

July 8, 2010

[1]Ocean Chemistry Division, NOAA/AOML, 4301 Rickenbacker Causeway, Miami FL 33149; 305-361-4379; e-mail: Rik.Wanninkhof@noaa.gov

[2]Woods Hole Oceanographic Institution, Woods Hole MA, 02543 USA; 508-289-3776; email: sdoney@whoi.edu

[3]Ocean Climate Research Division, NOAA/PMEL, 7600 Sand Point Way NE, Seattle WA 98115; 206-526-6741; e-mail: John.L.Bullister@noaa.gov

[4]School of Oceanography, Box 357940 University of Washington, Seattle WA 98195; email: warner@u.washington.edu

[5] Environmental Physics, Institute of Biogeochemistry and Pollutant Dynamics, ETH Zurich, 8092 Zurich; email: nicolas.gruber@env.ethz.ch

[*] Now at: O.E.B. Department Harvard University, Cambridge MA 02138; email: nlevine@oeb.harvard.edu

Abstract

Repeat observations along the meridional Atlantic section A16 from Iceland to 56°S show substantial changes in the total dissolved inorganic carbon (DIC) concentrations in the ocean between occupations from 1989 through 2005. The changes correspond to the expected increase in DIC driven by the uptake of anthropogenic CO_2 from the atmosphere, but the ΔDIC is more varied and larger, in some locations, than can be explained solely by this process. Concomitant large changes in oxygen (O_2) suggest that processes acting on the natural carbon cycle also contribute to ΔDIC. Precise partial pressure of CO_2 measurements suggest small but systematic increases in the bottom waters. To isolate the anthropogenic CO_2 component, ΔC_{anthro} from ΔDIC, an extended multi-linear regression (eMLR) approach is applied along isopycnal surfaces. This yields an average depth-integrated ΔC_{anthro} of 0.53 ± 0.05 mol m^{-2} a^{-1} with maximum values in the temperate zones of both hemispheres and a minimum in the tropical Atlantic. A higher decadal increase in the anthropogenic CO_2 inventory is found for the South Atlantic compared to the North Atlantic. This anthropogenic CO_2 accumulation pattern is opposite to that seen for the entire Anthropocene up to the 1990s. This change could perhaps be a consequence of the reduced downward transport of anthropogenic CO_2 in the North Atlantic due to recent climate variability. Extrapolating the results for this section to the entire Atlantic basin (63°N to 56°S) yields an uptake of 5 ± 1 Pg C $decade^{-1}$, which corresponds to about 25% of the annual global ocean uptake of anthropogenic CO_2 during this period.

1. Introduction

Changing atmospheric composition, winds, temperature, and freshwater cycling are affecting the oceans on decadal timescales, but systematic observations of resulting changes in oceanic heat and freshwater content, as well as carbon, oxygen, nutrient, and transient tracer concentrations are few. The major objective of the CLIVAR/CO_2 repeat hydrography program (http://ushydro.ucsd.edu/; http://www.clivar.org/carbon_hydro/) is to observe and quantify these changes throughout the water column by re-occupying select ocean transects sampled in the previous one to two decades as part of the Joint Global Ocean Flux Study (JGOFS) and World Ocean Circulation Experiment/World Hydrographic Programme (WOCE/WHP) [*Wallace,* 2001]. Of particular interest are changes in total dissolved inorganic carbon (DIC) inventories in response to the uptake of anthropogenic CO_2 by the ocean.

Such observations will serve to better determine the fate of the anthropogenic CO_2 emitted into the atmosphere due to human activities. These observations can provide constraints for the net carbon flux of the terrestrial biosphere [*Sarmiento and Gruber,* 2002; *Sabine et al.,* 2004; *Le Quéré et al.,* 2009]. The measurements are used to challenge and evaluate numerical ocean models employed to assess the response of the ocean to increasing atmospheric CO_2 levels. The models are a powerful means to investigate the impact of variability on the ocean carbon cycle and consequently DIC levels in the ocean interior [*Levine et al.,* 2008]. Most models suggest that the ocean will remain the largest sustained sink for anthropogenic CO_2 over the next century [*Solomon et al.,* 2007]. However, ocean models differ appreciably in the future uptake of the ocean for different CO_2 emission scenarios due to different levels of uptake for a fixed climate and a given atmospheric CO_2 concentration and because of changes in the oceanic carbon cycle in response to changes in climate [*Friedlingstein et al.,* 2006; *Plattner et al.,* 2008].

A key question that must be addressed through observations and modeling is if there are feedbacks that will affect the uptake capacity of the ocean in response to atmospheric CO_2 increases and climate change [*Sarmiento and Le Quéré,* 1996; *Joos et al.,* 1999; *Lovenduski et al.,* 2007, 2008; *Le Quéré et al.,* 2007]. Therefore, sustained systematic oceanic observations are warranted (see, for instance, Figure TS.31, *Solomon et al.,* 2007; *IOC,* 2009).

A major accomplishment of the measurement campaigns of inorganic carbon, carbon isotopes, nutrients, and transient tracers in the ocean during the WOCE/WHP survey and the following synthesis effort was the production of a globally uniform dataset, GLODAP [*Key et al.,* 2004]. This dataset is used to estimate the inventory of anthropogenic carbon (C_{anthro}) in the ocean since the start of the industrial revolution (≈ AD 1750) sometimes referred to as the Anthropocene [*Crutzen and Steffen,* 2003]. Several different independent methods converged on a total C_{anthro} inventory in 1994 of 118 Petagram carbon (Pg C) ± 15-20% [*Sabine et al.,* 2004; *Waugh et al.,* 2006; *Khatiwala et al.,* 2009]. Appreciable differences exist between the methods for the total C_{anthro} inventory the Atlantic, with the ΔC* method suggesting a total inventory of about 47 ± 7 Pg C [*Lee et al.,* 2003] for a nominal year of 1994, relatively close to that suggested by *Waugh et al.* [2006] using a Transit Time Distribution (TTD) method. *Vazquez-Rodriguez et al.* [2009] found substantially higher inventories of 54 ± 8 Pg C on average south of 65°N, on the basis of a comparison of a larger range of methods, such as the C^0_{IPSL} [*Lo Monaco et al.,* 2005], TroCA [*Touratier and Goyet,* 2004], and φC_T [*Vazquez-Rodriguez et al.,* 2009] methods. However, their reported mean was driven upward primarily by the C^0_{IPSL}, a method that yielded a substantially higher inventory (67 Pg C) relative to the others (range of 48 to 55 Pg C). A careful assessment of the C^0_{IPSL} method, such as done for the ΔC* and TroCA methods [*Matsumoto and Gruber,* 2005; *Yool et al.,* 2010] will be required to constrain this number more conclusively. Nevertheless, most of the methods suggest a C_{anthro} inventory for the 1990s for the Atlantic of about 50 Pg C.

It is only recently that observational data on decadal changes of carbon content in the ocean have become available [*Sabine et al.,* 2004, 2008; *Peng et al.,* 2003, 2010; *Tanhua et al.,* 2007; *Murata et al.,* 2008; *Perez et al.,* 2008; *Brown et al.,* 2010]. However, none of these works have estimated the decadal uptake along a meridional section for the entire Atlantic basin. Studies of changing O_2 levels in the thermocline [*Emerson et al.,* 2001; *Matear et al.,* 2000; *Johnson et al.,* 2005; *Stramma et al.,* 2008, 2010] suggest that aside from changes in DIC due to penetration of anthropogenic CO_2, appreciable additional changes in DIC are occurring on decadal timescales in the intermediate and deep waters due to changes in remineralization and ventilation rates, and water mass movement. [Note, in this manuscript we define ventilation loosely as the process by which water, which is exposed to the atmosphere, is transferred from the surface mixed layer to the interior ocean]. These decadal regional physical and

biogeochemical changes are often correlated with large-scale climate reorganizations such as the El Niño-Southern Oscillation (ENSO), the Pacific Decadal Oscillation (PDO) [*Dore et al.,* 2003; *Brix et al.,* 2004; *Keeling et al.,* 2004], Southern Annular Mode (SAM) [*Lovenduski et al.,* 2007], and the North Atlantic Oscillation (NAO) [*Gruber et al.,* 2002; *Bates,* 2007; *Bates et al.,* 2002; *Thomas et al.,* 2008; *Watson et al.,* 2009; *Levine et al.,* The impact of the North Atlantic Oscillation on the uptake and accumulation of anthropogenic CO_2 in the North Atlantic Ocean thermocline, submitted to *Global Biogeochemical Cycles,* 2010]. On smaller scales, movement of fronts, isopycnal heave, "slosh" and eddies can also cause appreciable differences in concentrations on seasonal to decadal scales [*Rodgers et al.,* 2009]. With only infrequent water column measurements, the persistence and frequency of changes can only be inferred from general knowledge of ventilation and remineralization patterns, and water mass movement. Models can aid in interpretation of signals [*Levine et al.,* 2008; *Doney et al.,* 2006; *Rodgers et al.,* 2009; *Thomas et al.,* 2008].

The focus of the present study is to determine changes in DIC and C_{anthro} using data obtained along the meridional A16 section between nominally 20°W and 32°W in the Atlantic Ocean from Iceland to 54°S in the Southern Ocean (Figure 1). The Atlantic Ocean is of particular interest as, compared to its size, it has disproportionately taken up more CO_2 than the other basins due to the strong meridional overturning circulation and associated deep-water formation in the North Atlantic [*Lee et al.,* 2003; *Sabine et al.,* 2004]. The deep penetration of transient tracers [*Doney et al.,* 1998; *Körtzinger et al.,* 1999; *Tanhua et al.,* 2006] and C_{anthro} [*Gruber,* 1998; *Lee et al.,* 2003; *Tanhua et al.,* 2007; *Vazquez et al.,* 2009] in the North Atlantic compared to other basins are clear indications that uptake of anthropogenic CO_2 is controlled by water transport rather than air-sea transfer [*Sarmiento et al.,* 1992]. The current study shows that the anthropogenic CO_2 imprint is not simply a signal superimposed on a steady state background but that there is significant variability in the natural carbon cycle on decadal timescales, mostly in the upper 2000 m of the Atlantic Ocean, as manifested by variation in inorganic nutrients and O_2. The changes in nutrients and O_2 suggest changes in mixing, ventilation, and remineralization of organic carbon that will reflect in inorganic carbon levels as well.

Anthropogenic CO_2 is not a property that can be directly observed but rather must be diagnosed from DIC and other biogeochemical properties. Together with natural variability, this makes the quantification of decadal temporal trends in anthropogenic CO_2 in the ocean

challenging, and the inferred amount of anthropogenic CO_2 is dependent on the method of determination. The common approach for separating the anthropogenic CO_2 signal from the measured DIC assumes that there is a temporally invariant background concentration of DIC and nutrients along isopycnal surfaces that reflect the transport and mixing of "preformed" quantities. Superimposed on this background signal are concentrations of DIC and nutrients from the remineralization of organic matter and dissolution of calcium carbonates. The C_{anthro} is determined as the difference between the expected increase in DIC based on increases in nutrients and oxygen and measured DIC. Constant stoichiometries (Redfield ratios) between nitrate (NO_3^-), oxygen (O_2), and DIC are assumed to determine the remineralization component. The method was first proposed by *Brewer* [1978] and *Chen and Millero* [1979], and improved upon by *Gruber et al.* [1996]. These preformed approaches are used primarily to estimate the total anthropogenic CO_2 in the ocean, C_{anthro}. They have some shortcomings for estimating temporal changes in anthropogenic CO_2 over shorter intervals, ΔC_{anthro} [*Levine et al.*, 2008], largely because some of the underlying assumptions are not well met on shorter time-scales. For example, the stoichiometric ratios may not be constant, particularly in the thermocline of the North Atlantic [*Anderson and Sarmiento,* 1994] where some of the major changes in DIC are observed. Moreover, these approaches were not designed to detect changes in the preformed DIC values caused by changes in the air-sea gas transfer and mixing into the interior as these processes do not leave a "Redfieldian" remineralization imprint. In addition, oxygen changes due to ventilation will not be correlated with those of carbon through Redfield ratios but rather through ill-constrained mechanisms of water mass mixing and differences in gas exchange response times. The inability of these preformed techniques to separate changes due to remineralization from changes due to ventilation can lead to biased estimates of ΔC_{anthro}.

Another approach for separating temporal changes in anthropogenic carbon from natural DIC variability is through establishing relationships between DIC and variables linked to observed changes in DIC using multi-linear regressions (MLRs) [*Brewer et al.*, 1997; *Wallace,* 2001]. Applying these empirical relationships derived for the first time period to the hydrographic, nutrient, and oxygen data for the second time period and subtracting the resulting computed DIC values from the observations of DIC in the second time period yields a difference that is attributable to ΔC_{anthro}. Alternatively, in an approach called the extended multi-linear regression (eMLR), MLRs are created for the datasets of each of the time periods, and the two

regressions are differenced to determine another estimate of ΔC_{anthro} from the hydrographic, nutrient, and oxygen data from either of the time periods [*Friis et al.,* 2004; *Tanhua et al.,* 2007]. As the eMLR method uses the observed quantities at one time as independent variables rather than the changes in the quantities between two occupations, it provides a smooth spatial pattern of anthropogenic CO_2 changes in the ocean compared to the MLR method that shows more spatial variability in calculated ΔC_{anthro}. The MLR and eMLR methods implicitly assume that there are no appreciable temporal trends in the independent variables, and that the relationship between the dependent and independent variables remains the same except for carbon. This means that the MLR-based methods will not work over long periods when, for instance, temperature increases in the ocean will come into play, resulting in temporal changes in the different variables with a relationship that will be different than those inferred from the spatial analysis. The MLR methods are generally not used in the upper 200 to 300 meters, which exhibit large seasonal changes in dependent and independent variables.

Transient tracers are a good means to determine ventilation ages and ventilation pathways. The increases in trichlorofluoromethane (CFC-11) and dichlorodifluoromethane (CFC-12) in the deep and intermediate waters over time show the continued penetration of the atmospheric anthropogenic signals. However, there are limitations in using CFC-11 and CFC-12 in a quantitative sense. Mixing processes complicate the use of these tracers to determine water mass ages, although approaches such as inferring transit time distributions [*Waugh et al.,* 2006] provide a means to better define the ages. The atmospheric source function of CFC-11 and CFC-12 are not ideal anymore for use as oceanic transient tracers as their atmospheric concentrations have stabilized and decreased after implementation of the Montreal Protocol. This results in non-unique solutions when back-calculating CFC-ages from concentrations of CFC in recently ventilated water masses.

However, qualitative use of these tracers in combination with other lines of evidence is a powerful means to assess the origin of changes in inorganic carbon in the Atlantic basin and to verify the different approaches to determine ΔC_{anthro}. Changes in partial pressure of CO_2 (pCO_2) along with CFC concentrations are useful to attribute the cause in changes in DIC in the deep waters of the Atlantic Ocean where increases in DIC are near or below detection limit. CFC-ages are used here as well to compare the different methods of estimating decadal changes in anthropogenic CO_2.

The Methods section describes the Atlantic Ocean A16 cruise data that are used along with an assessment of quality and adjustments made to the data. Next, there is a description of the large-scale features in subsurface salinity, DIC, AOU, NO_3^-, CFC-12 age, and silicate to show the chemical characteristics of the water masses along the meridional A16 section. This is followed by a description of temporal changes that are observed between the cruises in 1989/1993, and 2005/2003. The change in anthropogenic CO_2 is determined based on an eMLR approach along density surfaces, and the resulting ΔC_{anthro} is compared to the partial pressure of CFC-12 (pCFC-12). A comparison of variations of the application of the eMLR method, and back calculation methods correcting for remineralization [*Peng et al.,* 2003] to estimate ΔC_{anthro} is provided in the supplementary material. The decadal ΔC_{anthro} are extrapolated for the whole basin and compared with the total anthropogenic CO_2 in the basin from the results of *Lee et al.* [2003] and the decadal C_{anthro} changes derived from models.

2. Methods

The cruises discussed cover a key meridional section through the Atlantic (Figure 1) with measurements of inorganic carbon parameters, transient tracers, and nutrients. Collectively, the cruises are referred to as the A16 cruises: the 1993 Ocean Atmosphere Carbon Exchange Study (OACES N.ATL-93) and the 2003 CLIVAR/CO_2 cruises which extend from 63°N to 2°S cover the northern section, and the 1989 South Atlantic Ventilation Experiment (SAVE 5, SAVE 6/HYDROS4) and 2005 CLIVAR/CO_2 cruises are in the south (Table 1). Sampling and analysis of all parameters described were performed following standard protocols [*WOCE,* 1994; *DOE,* 1994] using certified reference materials whenever available. The analyses for the two time periods were done with similar (and sometimes the same) instrumentation and often by the same research groups, further assuring uniformity of measurement protocol. Biases are believed to be minimal based on comparison of parameters in deep-water for the cruises in 1989, 1993, 2003, and 2005. The SAVE 5 and SAVE 6/HYDROS 4 cruises in 1989 are used instead of the OACES S.ATL-91 cruise in the South Atlantic. The SAVE cruises had full water column coverage of relevant parameters at 0.5 to 1° spacing extending from the equator to 56°S, while the OACES S.ATL-91 cruise coverage had 2° spacing for the full water column, alternating with stations down to 1000 m. Moreover, the southern terminus of the OACES S.ATL-91 cruise was at 42°S. The SAVE cruises used somewhat different protocols from the later cruises and, to

check for consistency, deep-water carbon data from the SAVE cruises were compared with the OACES effort in 1991 over the region where the cruise tracks overlapped. No statistically significant offsets were observed in DIC for the deep water between the cruises [*Wanninkhof et al.*, 2003].

The carbon, oxygen, and nutrient data of the earlier cruises (1989, 1993) were checked for consistency through extensive regional and cross-over comparisons in efforts such as GLODAP [*Gouretski and Jancke*, 2001; *Key et al.*, 2004; *Wanninkhof et al.*, 2003]. The quality and offsets of CLIVAR/CO_2 2003 and 2005 cruise data were scrutinized in the Carbon in the North Atlantic (CARINA) effort [*Key et al.*, 2010]. No significant offsets were determined for the datasets except for the O_2 and NO_3 data. The OACES N.ATL-93 O_2 data were systematically 7.5 µmol/kg too low [*Castle et al.*, 1998]. All O_2 data from the OACES N.ATL-93 cruise were corrected by this amount. We determined significant differences in deep water nitrate between the earlier (1989, 1993) and later (2003, 2005) cruises. Therefore, a correction factor of 0.996 and 0.982 was applied to all the published OACES N.ATL-93 and SAVE nitrate data, respectively, in order to reach better agreement with deep-water nitrate values measured on the CLIVAR/CO_2 2003 and 2005 endeavors. Phosphate data were missing for some of the earlier cruises and, therefore, PO_4 was not used in the analyses.

Station spacing was 0.5 degrees in latitude with samples taken at 34 to 36 depths using nominally 10 L-bottles, except for the OACES N.ATL-93 cruise where stations were occupied at 1-degree intervals with samples taken at 24 depths. Full profiles of inorganic carbon parameters and chlorofluorocarbon (CFC) were obtained on every full-degree station, and partial profiles were taken at the half-degree stations. Oxygen, salt, and nutrient samples were obtained from every sample bottle. Vertical sample spacing ranges from 20 m in the surface mixed layer to 300 m in the deep ocean where little variability is encountered. For the 2003 and 2005 cruises, two fixed, alternating sampling depths for adjacent stations were used. For the earlier cruises, sampling was adjusted to capture specific features in the water masses. To perform comparisons between the two time periods, data were gridded on a 1 degree by 50-m grid with an inverse-distance weighting scheme using a commercial software package (Surfer v. 7, Golden Software). This produced a gridded product that had about four times as many output values as the original chemical analyses. Close inspection suggests that the gridded products adequately represent the measurements. Maximum gridding artifacts determined from comparing measured values with

the overlapping grid output were 1.4 μmol kg^{-1} for DIC and 0.4 μmol kg^{-1} for NO_3^-. The largest differences were observed in the upper thermocline where there are steep concentration gradients of chemical parameters with depth.

High quality CFC-11 and CFC-12 analyses were performed during all cruises and are used as ventilation tracers to discern pathways of penetration of atmospheric constituents into the thermocline and deep ocean. Chlorofluorocarbons are man-made with a well-defined atmospheric input history with significant releases commencing in the 1940s. CFC levels have been used to infer decadal ΔC_{anthro} directly [*McNeil et al.,* 2002] and the C_{anthro} transient [*Khatiwala et al.,* 2009], but this requires some assumptions on uptake of CFC compared to CO_2. Chlorofluorocarbon levels in the water column are expressed in terms of their partial pressure or as CFC-ages. The CFC-12 age provides an estimate of the time the water parcel has been isolated from the atmosphere [*Doney and Bullister,* 1992]. The method assumes that the partial pressure of CFC (pCFC) in the surface water is the same as in the atmosphere when the water is isolated from the surface. The pCFC = [CFC]/K_0 where [CFC] is the concentration of CFC-11 or CFC-12 in the water and K_0 is the solubility of CFC-11 and 12 that is a function of temperature and salinity [*Warner and Weiss,* 1985]. The CFC-age is determined by matching the pCFC in the water with the time the atmosphere had the same pCFC. Mixing, particularly with water devoid of CFC, biases the CFC-age [*Doney et al.,* 1997]. Thus, while the CFC-age should not be interpreted as an exact match of water mass age, it is an indicator of the relative age of the water. CFC-12 age and pCFC-12 are used in the analyses as they have a slightly greater dynamic range because the CFC-12 concentrations in the atmosphere stabilized later than for CFC-11.

3. Large-Scale Subsurface Geochemical Features

The large-scale features in temperature, salinity, oxygen, and inorganic carbon along parts of this transect in the Atlantic have been described previously [for instance, *Tsuchiya et al.,* 1992, 1994; *Doney and Bullister,* 1992; *Lee et al.,* 1997; *Wanninkhof et al.,* 1999]. However, the referenced papers do not cover the entire section and do not include all parameters measured on the cruises described here, such that a brief description is provided focusing on the parameters used in the analysis. Figures 2a-f show north-south depth profiles of salinity, AOU, DIC, NO_3^-, SiO_2, and CFC-12 age for the CLIVAR/CO_2 cruises in 2003 and 2005.

The spatial patterns in the parameters are indicative of the large-scale water masses and transports. Near the surface, salinity is controlled by the difference in evaporation and precipitation with values exceeding 37 in the subtropics (Figure 2a). At higher latitudes, lower salinity values are encountered with a distinct asymmetry between the northern and southern latitudes. In the north, high salinity values (> 35) are found well into the thermocline down to 2000 m as a result of saline waters being advected northward by the Gulf Stream as part of the large scale meridional overturning circulation (MOC) and the inflow of saline Mediterranean intermediate water. The return flow of the MOC in the form of North Atlantic Deep Water (NADW) is seen as water with salinities >34.9 centered around 3000 m and is apparent as far south as 35°S. Northward transport of water originating in the Southern hemisphere is evident as the lower salinity water of the Antarctic Intermediate Water (AAIW) ($S \approx 34.8$) centered at about 1000 m and extending to 15°N. This well-defined water mass outcrops near 45°S and has been used in the first attempts to estimate anthropogenic carbon input into the ocean [*Brewer*, 1978; *Chen and Millero*, 1979]. Antarctic bottom water (AABW) with salinities less than 34.9 lie under the NADW and its features extend as far as 40°N.

The oxygen concentrations (Figure 2b) expressed as AOU are strongly affected by the large-scale transport patterns, as well as by ventilation, biological productivity, and remineralization. Low values indicate well-ventilated waters while high AOU are characteristic of waters with high remineralization and isolation from the atmosphere. The surface mixed layer shows negative AOU, indicating that O_2 is slightly supersaturated along the entire transect. All of the cruises occurred in the summer season, of their respective hemispheres, when near-surface oxygen supersaturation is common as a result of seasonal heating and net biological productivity producing O_2 [*Broecker and Peng*, 1982; *Shulenberger and Reid*, 1981], and possibly supersaturation due to bubble dissolution [*Thorpe*, 1984]. These processes exceed the rate of air-sea gas transfer of O_2 that drives the surface mixed layer towards saturation (AOU=0). Low AOU are observed in the NADW, suggesting exposure to the atmosphere within the last couple of decades. The profiles of transient tracers [*Doney et al.*, 1998] also show recent exposure to the atmosphere. This is manifested as low CFC-12 ages in Figure 2f. The low AOU signal in the NADW shows the same extent of southern penetration as the high salinity tongue discussed above (Figure 2a). The water of southern origin shows significantly higher AOU with the AABW having values well over 100 μmol kg^{-1}. The high AOU signal disappears north of the

Mid-Atlantic Ridge near the equator where waters of northern origin prevail, as indicated by the large decrease in SiO_2 (Figure 2e). This feature is accentuated as the northern part of the transect is east of the Mid-Atlantic Ridge where there is little AABW. High AOU values are also observed in intermediate waters from 50° to 35°S immediately below the core of the AAIW, which is the tongue of low salinity water. The high AOU values at the northern end of the AAIW (15°S to 25°N) are caused by high biological productivity in the overlying waters and long transit time from the AAIW outcrop regions in the Southern hemisphere. AOU with values over 220 μmol kg^{-1}, the highest AOU in the Atlantic basin along the A16 transect, are found at 400-700 m depth in the north tropical Atlantic due to these factors. This region also shows high NO_3^- values, but it lacks a strong SiO_2 signal (Figures 2d and 2e).

The spatial patterns in total dissolved inorganic carbon values (DIC) measured during the cruises of 2003 and 2005 (Figure 2c) are, in broad brush, similar to those of AOU, indicating that the same processes controlling AOU also affect DIC distributions. Well-ventilated waters of the NADW show low DIC despite their high salinity. The lowest subsurface DIC values are found at 1800-2000 m at high northern latitude. The two-dimensional view precludes assigning a definitive origin of the water, but based on the hydrography of the region it is likely eastward moving water originating from the Labrador Sea and Denmark Strait area. NADW, AAIW, and AABW are delineated in the same pattern as AOU. Of note are the very high DIC values of greater than 2240 μmol kg^{-1} in the undercurrents north and south of the equator at 400-700 m.

The spatial distribution of NO_3^- (Figure 2d) shows close similarities with those of AOU and DIC. The patterns are largely influenced by local remineralization and transport of waters with high preformed nitrate from the Southern Ocean [*Sarmiento et al.,* 2004, 2007]. The highest nitrate values are encountered at 500 m just north of the equator and are attributed to local remineralization. This can be inferred from the distribution in SiO_2 (Figure 2e) that does not show such maxima at these locations. Because of the slower water column remineralization of SiO_2, and substantial differences in the preformed values [*Sarmiento et al.,* 2007], it is a good tracer and separator of northern and southern component waters in the Atlantic [*Broecker and Peng,* 1982]. AABW has SiO_2 values over 100 μmol kg^{-1}, while NADW shows values in its core of about 20-30 μmol kg^{-1}.

The isolation of the water masses from the atmosphere is reflected by increasing CFC-12 age with depth (Figure 2f). The oldest waters are encountered in the center of the eastern basin in the North Atlantic (≈ 15-30°N) with near-zero CFC-12 concentrations (CFC-12 age > 60 years) from 2000 m to the bottom. Similar CFC ages are encountered to the south as well but not in the bottom waters due to ventilation of the AABW. The DIC, NO_3^-, and AOU maxima in the thermocline north and south of the equator do not correspond with the oldest CFC ages but rather have ages ranging from 30-50 years. This indicates that the features are heavily influenced by local remineralization rather than solely isolation.

4. Decadal Changes in Subsurface Water

Seasonal variability is thought to have little effect on chemical parameters below the winter mixed layer, and changes in the thermocline therefore reflect primarily changes on annual to decadal scales. Rossby waves and other subseasonal perturbations contribute to the variability as well [*Rodgers et al.,* 2009]. Figures 3a-c show changes in salinity, AOU, and DIC over time between the cruises by subtracting the gridded data of the later cruises from the earlier ones. These parameters are chosen as key biogeochemical indicators of physical, biological, and anthropogenic changes. Below the mixed layer, salinity changes are believed to be primarily a function of changes in circulation, heave and movement of fronts. AOU changes are attributed to these factors as well, but also reflect changes in ventilation and remineralization of organic matter. DIC is affected by all these processes plus increases due to the uptake of anthropogenic CO_2 from the atmosphere.

Increases in salinity are particularly pronounced down to 1000 m at high northern latitudes (40-60°N). This is attributed to the recovery of the large salinity anomaly that occurred in the early 1990s [*Belkin,* 2004]. There is also a substantial increase in salinity over the last decade near the surface (0-400 m) from 25°S to 42°S. The areas with decreasing salinity over the last decade are less pronounced in spatial extent. Significant decreases are observed in the North Atlantic from 5°N to 35°N down to about 500 m contrary to the longer term trend of salinity increases from 20°N to 50°N [*Stott et al.,* 2008] and freshening of the polar and subpolar region [*Curry and Mauritzen,* 2005]. The intertropical convergence zone (6°N-9°N) shows large increases in salinity. The freshening of the tropics and subtropics corresponds to an overall weakening of the NAO between 1993 and 2003 [*Stott et al.,* 2008] and the associated decreased

transport of salty Gulf Stream water into the region. The increased salinity in the intertropical convergence zone is attributed to the drought in Amazonia during 2002-2006, causing a large reduction in precipitation and river flow into the north tropical Atlantic [*Marengo et al.,* 2008].

Changes in AOU are shown in Figure 3b. Most of the large differences in AOU (> |5| μmol kg^{-1}) are concentrated in the upper 1000 m. Large increases in AOU are seen at 700-1000 m depth from 40-60°N, and decreases are apparent nearer to the surface. *Johnson et al.* [2005] and *Johnson and Gruber* [2007] performed a detailed analysis of oxygen levels in the northeast Atlantic from 1988-2003, including the 1993 and 2003 data described here. They found that the changes are consistent with a northward movement of Mediterranean Outflow Water with high AOU since 1993 and a general contraction of the subpolar gyre. Increased ventilation of subpolar Mode Water at 0-500 m causes the observed decrease in AOU between observations. AOU increases at 500-1000 m in the region from 40 to 50°S and at 300-500 m from 16 to 20°N. There are decreases in AOU levels just north of these regions. Other areas of decrease in AOU are near the surface (50-300 m) from 5°N to 8°N and two regions of decrease in the Southern hemisphere with one at 300-600 m centered at 8°S and the other broad region at 300-600 m from 18°S to 25°S in the subtropical gyre. While the causes of these changes are not fully understood, the trends signify appreciable decadal variability in ventilation, circulation, and biogeochemistry in the Atlantic basin in the 1990s.

Changes in DIC (Figure 3c) correspond closely with the AOU anomalies (Figure 3b) but with substantially more positive anomalies in the surface water. The similarities and equal sign of the subsurface spatial patterns indicate that much of the temporal changes in DIC are related to changes in remineralization and ventilation that effect both carbon and oxygen, and shifts in water mass boundaries that act on the (natural) DIC and AOU gradients rather than on anthropogenic CO_2. These changes can occur by two mechanisms: 1) local increases in remineralization due to increasing rain rates of organic material; or 2) changes in circulation that draws water with different AOU and DIC into the region. We disregard here the contribution of changes in the dissolution of mineral $CaCO_3$, as the relative contribution of this process to gradients in DIC is much smaller than that of organic carbon [*Gruber and Sarmiento,* 2002; *Chung et al.,* 2003]. Changes due to circulation and remineralization are difficult to separate, but models, analysis of stoichiometric ratios, and other pieces of evidence, such as CFC data, suggest that changes in ventilation and water mass movement, such as caused by heave, play a dominant

role in the changes observed in DIC and AOU [*Johnson and Gruber,* 2007; *Levine et al.,* 2008; *Rodgers et al.,* 2009].

Salinity anomalies also contribute to the observed differences in DIC between the two time periods. To first-order, the magnitude of the changes in DIC due to freshwater dilution or concentration can be assessed though salinity normalization. The DIC values are normalized to the salinities observed in 2003/05 through: $DIC_{sal} = DIC \cdot Sal_{2003}/Sal_{1993}$. The maximum differences between DIC and DIC_{sal} range from -20 to 20 μmol kg^{-1}, and the patterns correspond, of course, exactly to the salinity anomalies shown in Figure 3a. The large differences in salinity, AOU, and DIC between the time periods clearly indicate that large changes in the natural DIC pool complicate the quantification of the ΔC_{anthro} signal in surface and intermediate waters, requiring sophisticated methods to separate the changes.

5. Deep-Water Changes in DIC and pCO_2

Decadal changes in deep water are more subtle than in the surface and intermediate waters, but detection of changes at depths below 2000 m are of relevance to estimate C_{anthro} inventories by virtue of the large volume of water [*Garzoli et al.,* 2010]. It is also important to discern possible anthropogenic influences and climate change signals at depth [*Johnson and Doney,* 2006]. Current reconstructions of C_{anthro} in the Atlantic based on ΔC^* show little penetration of C_{anthro} below 2000 m, except for the North Atlantic [*Gruber,* 1998; *Lee et al.,* 2003; *Sabine et al.,* 2004]. Other approaches show deep penetration at high southern latitudes as well [*Vasquez-Rodriguez et al.,* 2009], but these studies do not show appreciable deep water C_{anthro} in the interior away from high latitudes. The deep ocean C_{anthro} reconstructions are associated with substantial uncertainties, and C_{anthro} estimates of less than 5 μmol kg^{-1} are not considered very reliable [*Gruber et al.,* 1996]. Furthermore, *Matsumoto and Gruber* [2005] showed that there is a tendency for the ΔC^* method to underestimate deep ocean C_{anthro} levels. Several lines of evidence suggest a penetration of C_{anthro} into the deep Atlantic. *Körtzinger et al.* [1999] and *Wallace et al.* [1994] have shown measurable carbon tetrachloride CCl_4 in the deep Atlantic Ocean. This compound has no significant natural sources, and human emissions of CCl_4 started in the early 1900s compared to CFC emissions that commenced at significant quantities after 1940. While hydrolysis of CCl_4 and other removal mechanisms, particularly in thermocline [*Wallace et al.,* 1994], precludes its use as a robust age tracer, the presence of CCl_4 implies that

443 C_{anthro} has penetrated to these depths. *Johnson and Doney* [2006] detected small changes in
444 temperature in AABW in the South Atlantic along the A16 transect over the last decade that
445 might be due to anthropogenic climate change. *Brown et al.* [2010] using three cruises along the
446 24.5°W (A5) transect in 1992, 1998, and 2004 suggest small increases (≈ 2 μmol kg^{-1}) in C_{anthro}
447 in the bottom water. *Perez et al.* [2008] suggest similar small increases in the Irminger Sea
448 between 1983 and 2003.

449 With measurement uncertainties in DIC of ±2 μmol kg^{-1} and expected decadal DIC
450 changes driven by changes in anthropogenic CO_2 in deep water comparable to this level, it is
451 difficult to attribute quantitatively ΔC_{anthro} in deep water on decadal timescales. However,
452 changes in DIC can be deduced from other inorganic carbon parameters, such as the subsurface
453 partial pressure of CO_2, which was measured on all cruises. The partial pressure of CO_2
454 measured at 20°C, $pCO_2(20)$, has about six times the dynamic range of DIC with comparable
455 precision [*Wanninkhof and Thoning*, 1993], thereby increasing the signal to noise ratio
456 substantially. While the changes in $pCO_2(20)$ over time are not a unique tracer of C_{anthro}, since
457 changes in remineralization will also affect $pCO_2(20)$, it can provide evidence of changes that
458 might be attributed to invasion of C_{anthro} when used in concert with other tracers.

459 Deep-water $\Delta pCO_2(20)$, which is the difference between the CLIVAR and WOCE cruise
460 $pCO_2(20)$, and shown as four-degree latitude averages for sigma-4 surfaces below 45.813 kg m^{-3}
461 (≈ > 3500 m), from 40°N to 40°S are given in Figure 4a. The corresponding values for ΔDIC
462 and ΔAOU are shown in Figures 4b and 4c, emphasizing the utility of $pCO_2(20)$ for detecting
463 changes in the deep ocean. The $pCO_2(20)$ shows a consistent increase of about 10 μatm $decade^{-1}$
464 over the time interval between cruises along this deep section except for 12-20°N and 12-16°S.
465 For the DIC and TAlk concentrations at these depths this corresponds to a change in DIC of 1.5
466 μmol kg^{-1} $decade^{-1}$ at constant TAlk. The regions between 12-20°N show both smaller
467 $\Delta pCO_2(20)$ and larger variability as indicated by the larger standard error (Figure 4a) similar to
468 the changes in ΔAOU (Figure 4c). At southern latitudes greater than 32°S, the larger values of
469 ΔpCO_2 are consistent with the penetration pathway of the AABW, i.e., reflect younger waters
470 relative to those further north. The observed ΔDIC for each 4° bin scatter about 0 in deep water
471 (Figure 4b). The change in DIC corrected for changes in remineralization, ΔDIC_{O2} (see Eqn. A1
472 of the supplementary material for the definition of ΔDIC_{O2}), are systematically higher,
473 suggesting a DIC increase independent of remineralization processes. However, the increase is

small compared to the uncertainty in DIC measurements of about 2 μmol kg^{-1}. In the tropical North Atlantic (≈ 0 to 24°N), the AOU values have decreased slightly, which would lead to negative changes in ΔpCO_2 if the AOU decrease is caused by decreases in remineralization. Thus, the ΔpCO_2 attributed to anthropogenic CO_2 in the tropics might actually be slightly larger than observed in Figure 4a. Attribution of the signal to anthropogenic changes cannot be definitive, as small changes in either DIC or TAlk will have a pronounced effect on the $pCO_2(20)$. However, the combination of appreciable change in $\Delta pCO_2(20)$, together with detectable pCFC, little change in AOU, and small but predominant positive changes in ΔDIC_{O2}, suggests that decadal changes in C_{anthro} are occurring in the deep waters. Table 2 provides a summary of deep-water ΔpCO_2, ΔDIC_{O2}, ΔDIC, and $\Delta DIC_{eMLRdens}$ (see description below) of the northern section (> 15°N), the tropical, and southern sections (< 15°S) along with an average of the entire section. There is a section-wide increase in ΔC_{anthro} of 0.4-1.3 μmol kg^{-1} $decade^{-1}$ in deep-water (for $\Delta DIC_{eMLR\text{-}dens}$ and ΔDIC_{O2} estimates, respectively) but with an uncertainty of over 1 μmol kg^{-1} $decade^{-1}$. The ΔpCO_2 shows an average increase of 9.3 μatm $decade^{-1}$, and the consistently positive values affirm the small increases in ΔC_{anthro}. The northern section of the line covers the deep eastern basin, which belongs to the least ventilated deep basins of the entire Atlantic, and it correspondingly shows lower decadal changes.

6. Detecting Decadal Changes due to the Invasion of Anthropogenic CO_2

Among the many ways to estimate the change in anthropogenic CO_2 in the ocean, we have the greatest confidence in an approach called the extended multiple linear regression applied along isopycnal surfaces ($eMLR_{dens}$), in part because of the good correspondence with patterns of CFC penetration into the ocean. The $eMLR_{dens}$ method also tends to reduce the dynamic range of DIC values that need to be captured by the regression, reducing the absolute values of the residuals, and hence minimizing the uncertainty of the approach.

Issues with the decomposition of the ΔDIC signal can be minimized with an empirical multi-linear regression (MLR) approach [*Wallace,* 2001], which we apply in the extended form (eMLR) as described in *Friis et al.* [2004]. For the (single) MLR, a multi-linear regression is determined between DIC and a number of independent variables for time 1, t_1:

$$DIC_{MLR1,\,t1} = (a_1 + b_1\,SiO_{2t1} + c_1\,NO_{3t1} + d_1\,AOU_{t1} + e_1\,S_{t1} + f_1\,T_{t1}). \quad (1)$$

These coefficients, a_1-f_1, are then used with the independent variables for a later time, t_2, to calculate DIC at time t_2 ($DIC_{MLR1,\,t2}$). The difference between the calculated and observed DIC calculated for time t_2 (DIC_{t2}) is assumed to be the anthropogenic CO_2 increase:

$$\Delta DIC_{MLR} = DIC_{t2} - DIC_{MLR1,\,t2}$$
$$= DIC_{t2} - (a_1 + b_1\,SiO_{2t2} + c_1\,NO_{3t2} + d_1\,AOU_{t2} + e_1\,S_{t2} + f_1 T_{t2}). \quad (2)$$

In the eMLR, a second regression is performed for time 2, t_2:

$$DIC_{MLR2,\,t2} = (a_2 + b_2\,SiO_{2t2} + c_2\,NO_{3t2} + d_2\,AOU_{t2} + e_2\,S_{t2} + f_2\,T_{t2}). \quad (3)$$

ΔDIC_{eMLR} is then calculated by subtracting the DIC calculated for time t_2 using the t_1 regression parameters ($DIC_{MLR1,\,t2}$) from the DIC calculated for time t_2 using the t_2 regression parameters ($DIC_{MLR2,\,t2}$).

$$\Delta DIC_{eMLR} = DIC_{MLR2,\,t2} - DIC_{MLR1,\,t2}$$
$$= ((a_2-a_1) + (b_2-b_1)\,SiO_{2t2} + (c_2-c_1)\,NO_{3t2} + (d_2-d_1)\,AOU_{t2} + (e_2-e_1)\,S_{t2} + (f_2-f_1)\,T_{t2}) \quad (4)$$

The significance of each term is estimated from a stepwise regression of the independent parameters used in Eqns. 1 and 3. A stepwise MLR for the whole 1991 and 1993 dataset shows a decreasing ranking of importance to the fit from SiO_2, NO_3, S, T, to AOU. The correlation coefficient, r^2, increases from 0.61 and a root mean square, rms, error of 21 μmol kg^{-1} using a constant and SiO_2, to a r^2 of 0.97 with a rms error of 5.5 μmol kg^{-1} using all the parameters in Eqn. 1. For the section occupied in 2003 and 2005, the ranking is SiO_2, NO_3, AOU, S, and T with the r^2 increasing from 0.65 with a rms error of 21 μmol kg^{-1} using a constant and SiO_2, to a r^2 of 0.98 with a rms error of 4.5 μmol kg^{-1} using all the parameters in Eqn. 3. The difference in ranking of AOU, from the least important parameter for improving the MLR for the older dataset to the third most important parameter for the newer data, is attributed to lower quality of oxygen measurements for the older data.

The eMLR approach is applied along isopycnals based on the premise that this is the preferred pathway of water movement and penetration of anthropogenic CO_2 into the ocean [*Gruber et al.,* 1996; *Quay et al.,* 2007]. An isopyncal analysis framework also greatly damps the aliasing of natural variability caused by vertical heave [*Doney et al.,* 2007; *Levine et al.,* 2008]. Changes in biogeochemical parameters along isopycnals are mostly gradual. Coefficients for the MLR are determined for 23 isopycnal intervals along sigma-0, sigma-2, and sigma-4 surfaces using the same intervals proposed in *Gruber* [1998] and also applied by *Lee et al.* [2003] in their quantification of anthropogenic CO_2 in the Atlantic basin. When estimating water column changes in ΔC_{anthro}, we use the depth of the isopycnal surfaces for the 2005/2003 cruises to project the density coordinates back to depth coordinates. The uncertainties in the eMLRs range from 2 to 6 μmol kg^{-1} $decade^{-1}$ depending on the isopycnal surface, with higher residuals near the surface and lowest at mid-depth in the potential density (sigma-0) range of 26.8 to 27.3 kg m^{-3} (Table 3). The larger residual in the surface is attributed in part to temporal changes that are attributed to seasonal dynamics in the independent variables. In other efforts using the eMLR approach [*Friis et al.,* 2004; *Brown et al.,* 2010], the near-surface is excluded and data is extrapolated from the bottom of the winter mixed layer to the surface. However, since the eMLR is applied along isopycnals and because the cruises were performed in the same season, we believe that our approach to create a specific eMLR for the isopycnals up to the surface is preferable. For the very deep sigma-4 layers, limited data and small ranges of independent variables lead to increases in residual values. The average residual for all isopycnal surfaces between the calculated and observed DIC for the 1993/1989 data was 4.6 μmol kg^{-1} while that for the 2003/2005 data was 3.3 μmol kg^{-1}. The difference is attributed to less precise measurements and less coverage in the earlier era. As shown in Figure 3a, significant salinity differences were observed between the re-occupations that could change the density structure and thus impact the results of eMLR applied along isopycnals. Inspection of the changes in density structure for the isopycnal intervals used (Table 3) shows minimal changes for the two time periods in the gridded products used, and the changes in depth of isopycnals have no impact in the estimated inventories.

The $eMLR_{dens}$ distribution shows the expected pattern of high ΔC_{anthro} in the subtropical surface waters and deeper penetration near the outcrops, with decreasing levels towards the interior along isopycnal surfaces (Figure 5). It also shows some interleaving of higher and lower

ΔC_{anthro} differences between different density layers. Of note is the lower ΔC_{anthro} of ≈ 2-4 µmol kg^{-1} $decade^{-1}$ in the sigma-0 27.0 to 27.2 kg m^{-3} interval (≈ 600 m) compared to levels of ≈ 4-8 µmol kg^{-1} $decade^{-1}$ in the density horizons above and below in the Southern hemisphere. These patterns often show an inverse trend with AOU that was also observed in the North Atlantic in the analysis of *Friis et al.* [2004]. This lends support to the notion that the older water parcels, as suggested by higher AOU values, have lower ΔC_{anthro}. The maximum near-surface values occur in the subtropical gyres due to net convergence. This is in agreement with the finding that waters with low Revelle factors hold more anthropogenic CO_2 [*Sabine et al.*, 2004].

In the supplemental material, other estimates of ΔC_{anthro} are presented based on variations of the MLR approach. A key difference with the other methods (see Figure A2) is that penetration of the ΔC_{anthro} signal in the AABW to the bottom is absent in the $eMLR_{dens}$ analysis. CFC levels are low in the AABW at depth, and appreciable ΔC_{anthro} in this water mass would not be expected. As described above, the deep-water shows changes in $pCO_2(20)$ that correspond to changes of less than 2 µmol kg^{-1} $decade^{-1}$ (Figure 4b; Table 2). However, it is at depth in high southern latitudes that the various methods to determine C_{anthro} differ significantly as well [*Vasquez-Rodriguez et al.*, 2009], suggesting some caution in interpreting this ΔC_{anthro} signal, or absence thereof, in this region.

7. Comparison of ΔC_{anthro} Trends with Transient Tracers

To assess the fidelity of the $eMLR_{dens}$ method of estimating ΔC_{anthro}, we compare the results with chlorofluorocarbon (CFC) measurements. Changes in CFC-11 or CFC-12 could, in principle, be used to assess changes in penetration over the time period, as shown in *Doney et al.* [1998]. However, the CFC-11 and CFC-12 levels in the atmosphere have stabilized and decreased in recent years, complicating the interpretation of trends in the upper ocean over the last decade. In addition, mixing of CFCs in the ocean affects the CFC distributions in non-linear fashion and can have a significant effect on the interpretation of differences between time periods [*Waugh et al.*, 2006]. As a result, no strong correlations are found between changes in CFC over the time period and ΔC_{anthro}. However, there are characteristic trends between ΔC_{anthro} and pCFC that are diagnostic.

595 The comparison between ΔC_{anthro} and CFC concentrations is done in terms of partial
596 pressure of CFC-12, pCFC-12, to avoid misrepresentation due to the solubility dependence of
597 CFC concentrations. Figure 6 shows the trends of $\Delta DIC_{eMLRdens}$,which is the ΔC_{anthro} calculated
598 by the eMLR applied along isopycnals, versus pCFC-12 for the depth range of 250-2500 dB.
599 There is a general increase in ΔC_{anthro} with increasing pCFC-12 but with significant scatter that is
600 attributed to several factors: the time histories of pCFC and anthropogenic CO_2 in the
601 atmosphere are different, with the pCFC-12 increases occurring over a much shorter period
602 starting after about 1945 with a rapid increase till the mid-1980s and stabilizing in the mid-
603 1990s. In comparison, the atmospheric CO_2 growth rate has increased monotonically over this
604 time period such that mixing of water will cause a non-unique pattern of ΔC_{anthro} and pCFC-12.
605 The rapid increase of ΔC_{anthro} at low pCFC-12 in Figure 6 is attributed to mixing of water
606 containing ΔC_{anthro} and pCFC-12 with older water that is free of CFC but contains appreciable
607 anthropogenic CO_2. To highlight the different trends in the Atlantic basin, the data are separated
608 in regions poleward of 15°N and 15°S and the tropical area. The $\Delta DIC_{eMLRdens}$ (Figure 6) shows
609 a rapid increase of anthropogenic CO_2 at low pCFC-12 (≈ 0-80 ppt) in the Southern hemisphere
610 that is attributed to mixing of older waters as described above. The southern waters show slightly
611 greater ΔC_{anthro} for a given pCFC than the northern section except for CFC-12 values between
612 300 and 500 ppt, which are associated with shallow AABW. The trends in the Southern
613 hemisphere suggest a complicated mixing and penetration pattern of anthropogenic CO_2.

614 The northern section trend is more homogeneous and is attributed to more rapid mixing
615 along the isopycnals [*Doney and Bullister,* 1992; *Doney et al.,* 1997]. The negative $\Delta DIC_{eMLRdens}$
616 in the interior of the northern section suggests that the $eMLR_{dens}$ technique does not fully capture
617 ΔC_{anthro}, as no systematic negative ΔC_{anthro} values would be expected with the eMLR approach.
618 Thus, the water column inventory might be underestimated at low latitudes. The equatorial area
619 shows both patterns of Northern and Southern hemispheres because waters from northern and
620 southern origins impact the region. The maximum values of $\Delta DIC_{eMLRdens}$ agree with expected
621 net increases in ΔC_{anthro} in surface water of 6-10 μmol kg^{-1} $decade^{-1}$ if the DIC in surface water
622 keeps up with atmospheric CO_2 increases. The other approaches to determine ΔC_{anthro} discussed
623 in the supplementary material show trends with pCFC-12 and ΔC_{anthro} that differ from what
624 would be expected based on their atmospheric input histories (see Figure A4, supplementary
625 material).

To further assess the fidelity of the $\Delta DIC_{eMLRdens}$ method, we show the spatial distribution of this parameter along with other diagnostics on a sigma-0 surface of 27.3 kg m^{-3} in Figure 7. This isopycnal surface of AAIW outcrops at high latitudes reaches a maximum depth of 1100 m in the South Atlantic subtropical gyre and continues at 700-800 m depth in the North Atlantic up to 45°N where it shoals rapidly (Figure 7a, right axis). CFC-12 ages (Figure 7a, left axis) show a progressive aging from high latitude to a maximum tracer age of 55 years at 10°N and 10°S. Given the CFC-12 atmospheric time history, computed CFC-12 tracer ages have a maximum bound of about 60 years, and the actual mean ages along this isopycnal in the tropics are likely higher. Along the equator there appears to be some ventilation and/or mixing, with ages decreasing to 45 years likely due to the zonal undercurrents in this region. The DIC values (Figure 7b) for the 2003/2005 data progressively increase along the isopycnal towards the tropics, due to remineralization, with an increase of 110 µmol kg^{-1} in the northern tropical region and 70 µmol kg^{-1} in the southern tropical region compared to the southern outcrop region. It is of note that the DIC calculated from MLR_{dens} created from the 2003/2005 data (Eqn. 3) reproduce the observed DIC values very closely (Figure 7b). Figure 7b shows the challenge of estimating ΔC_{anthro} (< 10 µmol kg^{-1} $decade^{-1}$) superimposed on a large spatial range of DIC (≈ 50-100 µmol kg^{-1}). The $\Delta DIC_{eMLRdens}$ with coefficients specific to this density horizon (Table 3) shows larger changes nearer to the outcrop areas and spatial patterns roughly inverse to those of CFC-ages (see Figure 7a). However, the $\Delta DIC_{eMLRdens}$ values go negative for the oldest waters. There is a sharp salinity gradient along this isopycnal around 20-15°N, indicating a transition from warmer and saltier northern component water to older, colder, and fresher southern component water [*Broecker and Östlund,* 1979; *Kawase and Sarmiento,* 1985] that is also reflected by a rapid increase in CFC-age (Figure 7a). The density class in this region is likely formed by mixing of several different water masses that cannot be effectively captured by the $eMLR_{dens}$ method. This region also shows an increase of ≈ 4 µmol kg^{-1} $decade^{-1}$ in AOU [*Stramma et al.,* 2010], suggesting large biogeochemical changes that could impact the eMLR results. Overall, the $eMLR_{dens}$ approach provides an estimate of ΔC_{anthro} that is consistent with patterns of ventilation and magnitude, but regional biases are apparent.

8. Estimate of Total Inventory Change in the Atlantic Ocean

Estimates of decadal inventory changes of ΔC_{anthro} in ocean basins are few because of limited re-occupations to date, natural variability, and methodological challenges. The observations along the A16 line are believed to offer a reasonable whole basin estimate for the Atlantic as it transects the middle of the basin. As shown by *Gruber et al.* [1996], *Körtzinger et al.* [1999], *Tanhua et al.* [2006], *Vazquez-Rodriguez et al.* [2009], and *Brown et al.* [2010], the C_{anthro} signal penetrates deeper in the western basin of the North Atlantic compared to the eastern side, with the location of the A16 transect providing an approximate center line. *Murata et al.* [2008] shows higher decadal changes from 1994-2003 in the western basin than the eastern basin of the South Atlantic (30°S). The average specific inventory trend between 35°W and 15°W obtained by *Murata et al.* [2008] was 0.71 mol m^{-2} $year^{-1}$ in agreement with our $\Delta DIC_{eMLR\text{-}dens}$ estimate in the South Atlantic (> 15°S) of 0.76 mol m^{-2} $year^{-1}$ (Table A1). Their zonal estimate for 30°S is 0.6 mol m^{-2} $year^{-1}$. The comprehensive analysis by *Lee et al.* [2003] of the total inventory of C_{anthro} in the Atlantic, utilizing 17 cruises occupied during the WOCE/WHP, shows that the observations along the A16 line are representative of the basin average for the total increase of C_{anthro} during the Anthropocene.

Extrapolating the $eMLR_{dens}$ results from A16 using a volume weighted average and integrating over depth leads to a total basin inventory change of 1.9 Pg C for the North Atlantic from 1993 to 2003 (63°N-2°S), or 1.9 Pg C $decade^{-1}$, and 5.2 Pg C for the South Atlantic (54°S-2°S) for 1989-2005, or 3.0 Pg C $decade^{-1}$. Figure 8 shows a similar decadal uptake pattern over 10° latitude bands using the $eMLR_{dens}$ method compared to the total inventory for the Anthropocene as determined by *Lee et al.* [2003]. The inventory estimates from the $eMLR_{dens}$ approach show small inventories at low latitude and even negative inventory changes over the decade at 16°N. This is likely an artifact of the approach as described above in that the $eMLR_{dens}$ approach does not adequately capture the ΔC_{anthro} across fronts and mixing of water masses, as well as decadal trends of AOU in the region [*Stramma et al.*, 2010].

Assessing a robust error estimate is difficult due to a variety of systematic, compensating, and random errors involved in the assumptions and extrapolations. The residuals in the eMLR are 50 to 200% of the signal (Table 3) but these are random and Gaussian, and the standard error (defined as rms residual/(number of points)$^{0.5}$) is an order of magnitude smaller for the isopycnals where most of the change in inventory occurs. An estimate of the error for the entire basin is obtained by comparing results of different approaches. The different MLR approaches

686 summarized in Table A1 yield a specific inventory standard deviation along the section of 0.06
687 mol m^{-2} a^{-1} (with a mean of 0.6 mol m^{-2} a^{-1}) or about 10%. Following the analysis of *Lee et al.*
688 [2003], we double the uncertainty estimate, to include the uncertainties in the basinwide
689 extrapolation based on the uncertainty of C_{anthro} distribution, to a 20% overall uncertainty
690 (1-sigma) or 1 Pg C $decade^{-1}$.

691 The data-based inventory change compares well with model estimates. The basin-scale
692 uptake of 5 ± 1 Pg C $decade^{-1}$ for the last decade is similar to ΔC_{anthro} from the CCSM BEC
693 model [*Doney et al.*, 2009] for the Atlantic Ocean north of 64°S of 4.5 Pg C $decade^{-1}$ for the
694 period from 1993 to 2003. Using a suite of 10 ocean general circulation models, *Mikaloff*
695 *Fletcher et al.* [2006] estimate an inventory trend of 0.58 ± 0.1 Pg C $year^{-1}$ (5.8 ± 1.0 Pg C
696 $decade^{-1}$) for a nominal year of 1995. The estimate is based on an inversion of the ΔC^* inferred
697 inventory of C_{anthro} using the transport models to determine the magnitude and distribution of the
698 surface fluxes of C_{anthro} that are optimally consistent with that inventory.

699 A robust feature in our estimate that is not observed in model output is that the change in
700 the ΔC_{anthro} inventory in the South Atlantic of 3.0 Pg C $decade^{-1}$ is greater than in the North
701 Atlantic of 1.9 Pg C $decade^{-1}$. This shows up in all of the MLR methods (see supplementary
702 material, Table A1). The difference shows up in the specific inventory change as well, and thus
703 is not solely due to a difference in volume between the North and South Atlantic, with the South
704 Atlantic containing 56% of the total basin water volume. The greater decadal change in the
705 inventory of anthropogenic CO_2 in the South Atlantic is opposite from the hemispheric
706 difference in the total inventory of C_{anthro} over the Anthropocene, for which 60% is found in the
707 North Atlantic (Figure 8). The CCSM BEC model shows an even larger asymmetry with an
708 uptake in the North Atlantic of 3.4 Pg C $decade^{-1}$ and for the South Atlantic 1.1 Pg C $decade^{-1}$
709 from 1993-2003. Our results also differ from the ocean inversion results of *Mikaloff Fletcher et*
710 *al.* [2006], which also suggest an about equal distribution of anthropogenic CO_2 uptake between
711 the North and South Atlantic (2.9 ± 0.8 Pg C a^{-1} for the region from 58°S to the equator and 3.0 ±
712 0.7 Pg C a^{-1} from the equator to 76°N). The result is intriguing, particularly when combined with
713 the observation of *Quay et al.* [2007] based on ^{13}C isotopic evidence that a significant fraction of
714 C_{anthro} in the North Atlantic is transported from the south as opposed to supplied by local air-sea
715 gas transfer, a feature that is found only to a much smaller degree in the inversion results of
716 *Mikaloff Fletcher et al.* [2006].

This observation-based estimate suggests that the anthropogenic CO_2 uptake in the North Atlantic in the 1990s was less than the South Atlantic. Some of the difference could be because the observations were taken in the more poorly ventilated eastern basin in the North and better ventilated western basin in the South. However, the east-west asymmetry in tracers and C_{anthro} as observed by *Körtzinger et al.* [1999], *Tanhua et al.* [2006], and *Brown et al.* [2010] in the North Atlantic, and by *Murata et al.* [2008] in the South Atlantic is not large enough to account for differences determined. Another important caveat is that the inventory change in the North Atlantic is from 1993 to 2003, while the South Atlantic inventory change is determined from 1989 to 2005. As shown by *Brown et al.* [2010] and *Perez et al.* [2008], there are appreciable differences in observed C_{anthro} inventory changes on subdecadal timescales in the North Atlantic.

While speculative, the intensification of winds in the Southern Ocean causing upwelling of older waters leading to greater C_{anthro} uptake [*Lovenduski et al.*, 2008] and decreases in meridional overturning in the North Atlantic associated with a shift in the NAO in the mid 1990s [*Thomas et al.*, 2008; *Levine et al.*, The impact of the North Atlantic Oscillation on the uptake and accumulation of anthropogenic CO_2 in the North Atlantic Ocean thermocline, submitted to *Global Biogeochemical Cycles*, 2010] could both be factors resulting in increasing accumulation of C_{anthro} in the South Atlantic compared to the North Atlantic.

9. Conclusions

The CLIVAR/CO_2 repeat occupation of the WOCE/WHP line A16 shows significant water column changes in O_2 and DIC, particularly in intermediate waters, compared to cruises a decade earlier. The depth of the anomalies rule out seasonal variability. The $eMLR_{dens}$ method of estimating decadal changes in anthropogenic CO_2 in the water column yields a result of 0.53 ± 0.05 mol m^{-2} a^{-1} when integrated over the entire section. When extrapolated over the basin, the $eMLR_{dens}$ method yields an anthropogenic CO_2 increase of 5 ± 1 Pg C per decade from 63°N to 56°S, consistent with recent model results. The rate of accumulation of C_{anthro} is larger in the South Atlantic compared to the North Atlantic, which could be caused by recent patterns of climate variability and changes that alter the rate of transport of C_{anthro} from the surface ocean into the ocean's interior. The small changes in pCFC and pCO_2 in deep water taken a decade apart suggest that the anthropogenic CO_2 signal is penetrating into the bottom waters (>3500 m)

along this section. The pCFC-12 patterns are consistent with the depth distributions and regional patterns in ΔC_{anthro} derived using the $eMLR_{dens}$ approach.

Acknowledgments. The success and high data quality of the hydrographic cruises described are attributed to the dedication, professionalism, and skills of a multitude of seagoing personnel, crew, and officers of the UNOLS and NOAA research vessels. Their contribution is gratefully acknowledged. The CLIVAR/CO_2 cruises are co-sponsored by the physical and chemical oceanography divisions of the National Science Foundation and the Climate Observation Division of the Climate Program Office of NOAA. Support from the program managers involved is greatly appreciated. We also acknowledge a grant from NOAA (NOAA-NA07OAR4310098), which supported part of the post-cruise data analysis contributing to this manuscript. NG acknowledges support also from ETH Zurich. We appreciate the efforts of two anonymous reviewers who provided substantial comments that improved the manuscript. We wish to thank Gail Derr of AOML for copy editing and providing the camera ready manuscript.

Supplementary Material: Other Approaches to Estimate ΔC_{anthro} and Shortcomings

Here we compare several other approaches and permutations of the multiple linear regression MLR method to estimate temporal changes in ocean anthropogenic carbon ΔC_{anthro}. This comparison is performed to show the significant differences between approaches, which are larger at regional scale than when integrated over the entire Atlantic basin, suggesting that the biases in the methods partially cancel out over larger areas. First we describe the approaches based on correcting for changes in remineralization followed by empirical multi-linear regression methods.

One approach for estimating ΔC_{anthro} is to correct the observed changes in DIC, ΔDIC, for variations in organic remineralization using either AOU or NO_3^-, and $CaCO_3$ remineralization, using total alkalinity TAlk, and their stoichiometric (Redfield) ratios [*Peng et al.*, 2003]. The resulting ΔC_{anthro} estimates are denoted as ΔDIC_{O2} and ΔDIC_{NO3}, respectively. The inferred change due to anthropogenic CO_2 input, ΔC_{anthro}, over the period for this method is:

$$\Delta DIC_{O2} = \Delta DIC - R_{C:O}\,\Delta O_2 - 0.5\,(\Delta TAlk + R_{N:O}\,\Delta O_2) \quad \text{(A1)}$$

and:

$$\Delta DIC_{NO3} = \Delta DIC - R_{C:N}\,\Delta NO_3 - 0.5\,(\Delta TAlk + \Delta NO_3) \quad \text{(A2)}$$

where $\Delta DIC = DIC_{t2} - DIC_{t1}$, t_1 and t_2 are the earlier and later time periods, respectively, and ΔO_2, ΔNO_3^-, and ΔTAlk are defined in the same manner. $R_{C:O}$, $R_{N:O}$, and $R_{C:N}$ are the stoichiometric (Redfield) ratios of carbon and oxygen; nitrate and oxygen; and carbon and nitrate, respectively. The stoichiometric ratios of *Anderson and Sarmiento* [1994] are used, where P:N:C:O = 1:16:117:-170, yielding $R_{C:O} = -0.69$, $R_{N:O} = -0.094$, and $R_{C:N} = 7.31$. The third term on the right-hand side of equations A1 and A2 reflects the changes in DIC caused by dissolution of calcium carbonates. In the dissolution process, the alkalinity will increase two-fold faster than increase in inorganic carbon due to release of divalent carbonate ions, CO_3^{2-}. This term is adjusted for the decrease in alkalinity associated with increases in nitrate from remineralization of organic material [*Brewer*, 1978]. All quantities are corrected for changes in salinity over the time period by normalizing to salinities of t_2: $nX_{t1} = S_{t2}/S_{t1}\,X_{t1}$.

789 Basin-wide, there are no systematic decadal changes in alkalinity (M. Chanson *et al.*,
790 Synthesis and analysis of the carbonate parameters in the Atlantic Ocean based on decadal repeat
791 occupations of the meridional section, submitted to *Global Biogeochemical Cycles,* 2010), but
792 small regional changes in alkalinity, often correlated with salinity anomalies, are accounted for
793 in this method. For this method to provide reliable estimates of ΔC_{anthro}, it must be assumed that
794 the stoichiometric ratios are correct and invariant. Moreover, movement of boundaries of water
795 masses can lead to anomalous ΔC_{anthro} estimates, as changes in O_2 or NO_3 resulting from changes
796 in circulation and transport will be attributed to changes in remineralization.

797 Latitude-depth cross-sections for the ΔDIC_{O2} and ΔDIC_{NO3} approaches (Eqns. A1, A2)
798 are shown in Figure A1. There are several known issues with these approaches. *Anderson and*
799 *Sarmiento* [1994] derived the Redfield ratios from changes in intermediate and deep water in the
800 world's oceans assuming two-end member mixing. They excluded the North Atlantic because of
801 multi-end member mixing in this region, and because the ratios did not appear to be constant,
802 either because of issues with the separation of end members or because the remineralization
803 ratios are variable. In addition, both oxygen and nitrate have limitations as remineralization
804 parameters. Oxygen levels change both due to remineralization and changes in ventilation
805 processes that cannot *a priori* be separated [*Levine et al.,* 2008]. Nitrogen fixation [*Hansell et al.,*
806 2007] and possibly denitrification signals advected from the coastal margins, for which nitrate
807 levels are not in Redfield proportions to DIC, can bias the ΔDIC_{NO3} approach. Since there were
808 no absolute standards or certified reference materials for nitrate, biases between cruises that are
809 amplified by the $R_{C:N}$ of 7.31 can affect the results as well. Phosphate (PO_4) is, in principle, a
810 good remineralization tracer, as it is not affected by gas exchange or non-Redfieldian
811 decomposition, but the amplification of uncertainty due to the large $R_{C:P}$ of 117, along with poor
812 accuracy of PO_4 on some of the cruises, makes this parameter unsuitable for both the
813 remineralization and MLR methods for detecting ΔC_{anthro} on decadal timescales.

814 The ΔDIC_{O2} and ΔDIC_{NO3} approaches implicitly rely on stationary water masses, as the
815 decadal comparison assumes that the preformed ratios of carbon and nutrients at a particular
816 location do not change over time. On large scales, these are probably reasonable assumptions
817 but in frontal regions this can lead to regional biases. Vertical heave can also introduce biases
818 [*e.g., Rodgers et al.,* 2009]. The movement of fronts often shows up as large negative ΔC_{anthro}
819 anomalies adjacent to positive values. Figure A1a shows a banded pattern of ΔDIC_{O2}. This

suggests that the changes are related to oceanographic features with vertical structure, such as those associated eddies, Rossby wave and movement of fronts, that affect the patterns of ΔDIC_{O2}. Some changes can be attributed to changes in ventilation. The most obvious anomaly is the region of negative ΔDIC_{O2} at 40-55°N that corresponds to the areas with large O_2 decreases between 1993 and 2003 (Figure 3b) [*Johnson et al.*, 2005; *Johnson and Gruber*, 2007]. Other regions of negative ΔDIC_{O2} are in the Southern hemisphere near 46° and at 38°. The latter is associated with a large eddy [*Wanninkhof et al.*, 2006]. The remainder of the region shows generally positive changes but is patchy in nature. Integrating the ΔDIC_{O2} over the water column and averaging for the A16 line yields a water column inventory specific change of 0.82 mol m^{-2} a^{-1} that is higher than the simple difference in DIC over the time period (ΔDIC) of 0.58 mol m^{-2} a^{-1} (Table A1). Moreover, the spatial variability of ΔDIC_{O2} and ΔDIC is similar in scale and magnitude (see Figures 3c and A1), suggesting that the remineralization correction based on a stoichiometry of C:O of 117: -170 does not adequately reflect the ΔC_{anthro}.

The ΔDIC_{NO3} shows large regions of decrease near 20°N, 10°N, and the equator (Figure A1b). These decreases correspond with increases in NO_3^- for these regions (not shown) between the occupations in 1993 and 2003. There is no clear attribution for this pattern, and we believe it could be caused by station to station measurement biases during the cruises or changes in circulation patterns in the complex equatorial Atlantic current regime. The negative ΔDIC_{O2} at 40-55°N is not apparent in the ΔDIC_{NO3} field. Rather, it shows ΔDIC_{NO3} increases in the range of 5 to 10 µmol kg^{-1} that can be attributed to expected in-growth of ΔC_{anthro} over time in this well-ventilated region. This points towards a ventilation bias in ΔDIC_{O2} in this locale. The specific change in ΔDIC_{NO3} for the whole section of 0.39 mol m^{-2} a^{-1} is less than the average ΔDIC value of 0.58 mol m^{-2} a^{-1} with the major difference in the tropics, 15°N- 15°S (Table A1). The large absolute and regional differences between ΔDIC_{NO3}, ΔDIC_{O2}, and ΔDIC clearly show the large effect of the remineralization correction on the calculation of ΔC_{anthro}, and should serve as a caution using this approach to estimate decadal changes of anthropogenic CO_2 in the Atlantic Ocean.

The MLR and eMLR approaches assume that the independent variables are not affected by systematic trends, such as those caused by climate change, or at least not affected in a way that would alter their relationship amongst each other. The eMLR method gives a much smoother pattern for the change in DIC attributable to ΔC_{anthro} than the MLR method. This is

851 because the eMLR depends only on the absolute values of the independent variables, which have
852 small relative errors. Different independent variables can be chosen based on personal
853 preference, goodness of fit, linearity, data quality, and data availability. Here we assess the
854 effects of performing the MLR and eMLR for the whole basin and for select latitude bands. A
855 separate MLR analysis of this same dataset but using different independent variables is presented
856 in *Chanson et al.* (Synthesis and analysis of the carbonate parameters in the Atlantic Ocean
857 based on decadal repeat occupations of the meridional section, submitted to *Global*
858 *Biogeochemical Cycles*, 2010) with emphasis on the decadal changes in the coefficients and
859 goodness of fit.

860 Several different multi-linear regression (MLR) approaches are applied to the dataset to
861 show the sensitivity of the method to different assumptions. For these comparisons, the DIC was
862 regressed against T, S, AOU, NO_3^-, and SiO_2 in all approaches. Contrary to the $eMLR_{dens}$
863 analysis, data in the top 250 m are not used in developing the regressions to avoid biases due to
864 seasonality. Including the top 250 m increases the residuals by up to two-fold (from ≈ 4-5 µmol
865 kg^{-1} to 8-10 µmol kg^{-1}). The MLRs are created with either the 2003 and 2005 data or the 1989
866 and 1993 data. While the difference in time of occupation of the northern and southern sections
867 could affect the MLR, no apparent biases were found when checked against MLRs created for
868 each section separately. The approaches used are: the single MLR method utilizing the
869 1989/1993 data (Eqn. 1, main text) to create the regressions and applying the regressions to the
870 newer 2003/2005 data (Eqn. 2, main text); the eMLR method (Eqn. 4); and the eMLR method
871 applied separately to six latitude intervals (56 to 40°S; 40 to 15°S; 15 to 2°S; 2°S to 15°N; 15 to
872 40°N; and 40 to 63°N).

873 The single MLR utilizing the 1989/1993 data to create the regressions and applying the
874 regressions to the newer 2003/2005 data show ΔC_{anthro} increases of 5 to 10 µmol kg^{-1} centered at
875 a depth of about 1000 to 1500 m in the North Atlantic and South Atlantic (Figure A2a). There is
876 little change in the near-surface (≈ 250-500 m) waters of the subtropical gyres. A large area with
877 decreases of 5 to 10 µmol kg^{-1} is apparent in the intermediate waters from 35°S to 20°N. There
878 are increases of 5 to 10 µmol kg^{-1} in the deep water. The unanticipated negative changes, and
879 the increases in the deep water, are indicative of biases in the single MLR method that are, in
880 part, attributed to lower data quality of the older data used to create the MLR. This is apparent in
881 Figure A2b where the MLR are created with the 2003/2005 data and used to compare with the

1989/1993 data. In this analysis, the negative values in the intermediate water disappear. Higher ΔC_{anthro} are found near the surface with a maximum in the upper waters of the South Atlantic. There are also elevated values of 2 to 4 μmol kg^{-1} in the Antarctic Bottom Water (AABW) that might be attributable to rapid ventilation. However, there are also large negative anomalies at intermediate depths and in the bottom waters in the north that are clearly artifacts, putting the singe-MLR approach for the basin as a whole in doubt. The single MLR method can be refined by computing regressions separately for sub-basin regions [*Levine et al.*, 2008].

The eMLR approach (Figure A2c) shows smoother spatial patterns as would be expected by subtracting two linear regressions. The range of temporal changes is smaller, and the patterns of change in ΔC_{anthro} differ as well compared to the MLR and DIC_{O2} approaches. The spatial patterns are more uniform with highest levels near the surface and decreasing to zero by 2000 m. Near-surface values of 4-5 μmol kg^{-1} are lower than expected if the ocean uptake were to keep pace with atmospheric increases. No negative values are encountered, indicating that the biases in the single MLRs (Figures A2a and A2b) cancel out. Elevated levels are apparent in the AABW water at high southern latitudes, with values of 3 to 4 μmol kg^{-1}. While this is a ventilation pathway as shown by elevated CFC concentrations, the magnitude of change is large for these depths. These waters are characterized by high silica and nutrient concentrations and this might contribute to the bias of higher ΔC_{anthro} in these waters using the eMLR.

To determine if there are significant regional (or cruise differences) introduced by the MLR methods, separate MLRs were created for different sections roughly delineating subpolar, subtropical, and tropical gyres: 56 to 40°S; 40 to 15°S; 15 to 2°S; 2°S to 15°N; 15 to 40°N; and 40 to 63°N. The tropical region is split into two sections to separate the northern and southern cruises that occurred in different years. The sectional eMLR ($eMLR_{sectional}$) (Figure A2d) shows truncated ΔC_{anthro} values for AABW, with no penetration northward of 15°S, likely because of the separate regressions that are created for each region. However, no other large changes in the ΔC_{anthro} estimate due to truncating the eMLR at each regional boundary are apparent. The $eMLR_{sectional}$ shows higher values at depth at high latitudes and higher values in the subtropics than the eMLR for the whole section (Figures A2c and A2d). The sectional eMLR shows little change in ΔC_{anthro} in the tropical region and subpolar North Atlantic between 250 and 1000 m (Figure A2d).

912 Biases in the MLR approaches are assessed from the spatial patterns of the residuals
913 between the measured DIC and the calculated DIC, f(S, T, SiO_2, AOU, and NO_3^-), for the same
914 time period. Contour plots of the residuals are shown in Figures A3a-f. The spatial structure in
915 the residuals is non-random, which will affect the application of the MLRs to estimate ΔC_{anthro}.
916 Moreover, correlations between the independent variables can lead to biases. The whole section
917 of MLRs show the same pattern of spatial biases whether 1993 or 2005 data are used to create
918 the MLR, but the MLR created with 1993 data show slightly greater magnitudes of biases
919 (compare Figures A3a and A3b). The 2005 residuals are about a half of those of the 1993 data.
920 In both cases, the high latitudes and deep waters in the Northern hemisphere show positive biases
921 of 4-12 μmol kg^{-1} while intermediate water and subtropical surface waters show a negative bias
922 of similar magnitude. The eMLR approaches cancel out much of the residual structure. Using a
923 sectional eMLR in which the transect was divided into six latitude bands yields smaller residuals
924 ($eMLR_{sectional}$) (Figures A3e and A3f). The patterns are more horizontal and change sign at the
925 boundaries of the area with specific MLR. The MLR_{dens}, discussed in the main text, show the
926 smallest residuals with values of less than 4 μmol kg^{-1} (Table 3, Figures A3c and A3d). There are
927 no clear patterns in the residuals, although the Southern hemisphere shows predominantly small
928 negative biases and the Northern hemisphere shows positive offsets at depth.

929 A comparison of specific inventory estimates for the whole section, and for the North
930 Atlantic, equatorial Atlantic, and South Atlantic sections is provided in Table A1. The changes
931 are normalized to mol m^{-2} a^{-1} to account for the different times of occupation. A factor of two
932 difference in specific inventories is obtained for the different methods, largely due to regional
933 differences between the different methods, particularly in the equatorial Atlantic. In the
934 subtropical gyres in the North and South Atlantic, there is better correspondence between
935 methods. The high ΔDIC_{O2} values suggest that either the Redfield C:O ratios used are too high
936 for the North Atlantic [*Li and Peng,* 2002], or, more likely, that the net decrease of O_2 in the
937 North Atlantic thermocline in the 1990s biases the ΔC_{anthro} estimate determined by ΔDIC_{O2}. This
938 is in accord with observations of *Keeling and Garcia* [2002]. *Levine et al.* [2008] similarly find,
939 using a numerical model, that changes in O_2 due to ventilation and mixing significantly affect
940 estimates of ΔC_{anthro} using the ΔDIC_{O2} method. The lower values using the ΔDIC_{NO3},
941 particularly in the tropics, are attributed to biases in NO_3^- data or changes in currents.

A further check of the different methods to estimate ΔC_{anthro} can be performed by comparison with pCFCs. The ΔDIC_{O2} method shows no apparent trend with pCFC and gives a wide range of values (Figure A4a). The ΔDIC_{NO3} method has a similar random distribution (not shown). The ΔDIC_{eMLR} (Figure A4b) shows distinct, but different relationships between increasing anthropogenic carbon and pCFC for different regions. For the South Atlantic, a near-linear increase in ΔDIC_{eMLR} with pCFC is observed. The waters in the Northern hemisphere show two diverging trends. All waters between ≈ 200-500 db from 15 to 40°N, and the entire water column from 40 to 60°N, show a clear positive slope between ΔDIC_{eMLR} and pCFC. The deeper waters between 15°N to 40°N show approximately constant ΔDIC_{eMLR} of ≈ 1 μmol kg^{-1} for pCFC-12 varying from 0 to 250 ppt. This is because the pCFC decreases along isopycnal surfaces into the interior while the ΔDIC_{eMLR} as applied is a basin-wide regression that does not necessarily account for the pathways of transport. The data in the equatorial area lie between the northern and southern relationships, likely because the deeper water masses in this region do not form locally but are mixtures of northern and southern component waters.

The comparison of methods show large differences in ΔC_{anthro} for the whole section and, particularly, regionally. The methods show inconsistencies with respect to the residuals and when comparing the magnitudes with pCFC that cast doubt on the accuracy of the approaches. A rigorous set of diagnostics should be applied before inferring the ΔC_{anthro} from the approaches applied. The $eMLR_{dens}$ approach discussed in the main text appears the most robust empirical approach of determining decadal changes of anthropogenic CO_2 for the meridional section A16 in the Atlantic.

964 **References**

965 Anderson, L. A., and J. L. Sarmiento (1994), Redfield ratios of remineralization determined by
966 nutrient data analysis, *Global Biogeochem. Cycles*, *8*, 65-80.

967 Bates, N. R. (2007), Interannual variability of the oceanic CO_2 sink in the subtropical gyre of the
968 North Atlantic Ocean over the last 2 decades, *J. Geophys. Res.*, *112*, C09013,
969 doi:10.1029/2006JC003759.

970 Bates, N. R., A. C. Pequignet, R. J. Johnson, and N. Gruber (2002), Changes in the oceanic sink
971 of CO_2 in Subtropical Mode Water of the North Atlantic Ocean, *Nature*, *420*, 489-491.

972 Belkin, I. M. (2004), Propagation of the "Great Salinity Anomaly" of the 1990s around the
973 northern North Atlantic, *Geophys. Res. Lett.*, *31*, L08306, doi:10.1029/2003GL019334.

974 Brewer, P. G. (1978), Direct observation of the oceanic CO_2 increase, *Geophys. Res. Lett.*, *5*,
975 997-1000.

976 Brewer, P. G., C. Goyet, and G. Friederich (1997), Direct observation of the oceanic CO_2
977 increase revisited, *Proc., Natl. Acad. Sci. U.S.A.*, *94*, 8308-8313.

978 Brix, H., N. Gruber, and C. D. Keeling (2004), Interannual variability in the upper ocean carbon
979 cycle at Station ALOHA, Hawaii, *Global Biogeochem. Cycles*, *18*, GB4019,
980 doi:10.1029/2004GB002245.

981 Broecker, W. S., and H. G. Östlund (1979), Property distributions along the sigma theta = 26.8
982 isopycnal in the Atlantic Ocean, *J. Geophys. Res.*, *84*, 1145-1154.

983 Broecker, W. S., and T.-H. Peng (1982), *Tracers in the Sea*, Eldigio Press, Palisades, N.Y.

984 Brown, P. J., D. C. E. Bakker, U. Schuster, and A. J. Watson (2010), Anthropogenic carbon
985 accumulation in the subtropical North Atlantic, *J. Geophys. Res.*, *115*, C04016,
986 doi:10.1029/2008JC005043.

987 Castle, R., R. Wanninkhof, S. C. Doney, J. Bullister, L. Johns, R. A. Feely, B. E. Huss, F. J.
988 Millero, and K. Lee (1998), Chemical and hydrographic profiles and underway
989 measurements from the North Atlantic during July and August of 1993, *NOAA Data Rep*.,
990 ERL AOML-32, Springfield, N.J.

991 Chen, C.-T., and F. J. Millero (1979), Gradual increase of oceanic CO_2, *Nature*, *277*, 205-206.

992 Chung, S.-N., K. Lee, R. A. Feely, C. L. Sabine, F. J. Millero, R. Wanninkhof, R. M. Key, J. L.
993 Bullister, and T.-H. Peng (2003), Calcium carbonate budget in the Atlantic Ocean based on
994 water-column inorganic carbon chemistry, *Global Biogeochem. Cycles*, *17*, 1093,
995 doi:10.1029/2002GB002001.

996 Curry, R. G., and C. Mauritzen (2005), Dilution of the northern North Atlantic Ocean in recent
997 decades, *Science*, *308*, 1772-1774, doi:10.1126/science.1109477.

998 Crutzen, P. J., and W. Steffen (2003), How long have we been in the Anthropocene era? *Climatic*
999 *Change*, *61*, 251-257.

1000 DOE (1994), Handbook of methods for the analysis of the various parameters of the carbon
1001 dioxide system in sea water, version 2, *Rep. ORNL/CDIAC-74*, Oak Ridge Natl. Lab., Oak
1002 Ridge, Tenn.

1003 Doney, S. C., and J. L. Bullister (1992), A chlorofluorocarbon section in the eastern North
1004 Atlantic, *Deep-Sea Res.*, *39*, 1857-1883.

1005 Doney, S. C., W. J. Jenkins, and J. L. Bullister (1997), A comparison of ocean tracer dating
1006 techniques on a meridional section in the eastern North Atlantic, *Deep-Sea Res. I*, *44*, 603-
1007 626.

1008 Doney, S. C., J. L. Bullister, and R. Wanninkhof (1998), Climatic variability in ocean ventilation
1009 rates diagnosed using chlorofluorocarbons, *Geophys. Res. Lett.*, *25*, 1399-1402.

1010 Doney, S. C., K. Lindsay, I. Fung, and J. John (2006), Natural variability in a stable, 1000-yr
1011 global coupled climate-carbon cycle simulation, *J. Cli.*, *19*, 3033-3054.

1012 Doney, S. C., S. Yeager, G. Danabasoglu, W. G. Large, and J.C. McWilliams (2007),
1013 Mechanisms governing interannual variability of upper ocean temperature in a global
1014 hindcast simulation, *J. Phys. Oceanogr.*, *37*, 1918-1938.

1015 Doney, S. C., I. Lima, J. K. Moore, K. Lindsay, M. J. Behrenfeld, T. K. Westberry, N.
1016 Mahowald, D. M. Glover, and T. Takahashi (2009), Skill metrics for confronting global
1017 upper ocean ecosystem-biogeochemistry models against field and remote sensing data, *J.*
1018 *Mar. Syst.*, *76*, 95-112, doi:10.1016/j.jmarsys.2008.05.015.

1019 Dore, J. E., R. Lukas, D. W. Sadler, and D. M. Karl (2003), Climate-driven changes to the
1020 atmospheric CO_2 sink in the subtropical North Pacific Ocean, *Nature*, *424*, 754-757.

1021 Emerson, S., S. Mecking, and J. Abell (2001), The biological pump in the subtropical North
1022 Pacific Ocean: Nutrient sources, Redfield ratios, and recent changes, *Global Biogeochem.*
1023 *Cycles*, *15*, 535-554.

1024 Friedlingstein, P., P. Cox, R. Betts, L. Bopp, W. Von Bloh, V. Brovkin, P. Cadule, S. Doney, M.
1025 Eby, I. Fung, G. Bala, J. John, C. Jones, F. Joos, T. Kato, M. Kawamiya, W. Knorr, K.
1026 Lindsay, H. D. Matthews, T. Raddatz, P. Rayner, C. Reick, E. Roeckner, K. G. Schnitzler, R.
1027 Schnur, K. Strassmann, A. J. Weaver, C. Yoshikawa, and N. Zeng (2006), Climate-carbon
1028 cycle feedback analysis: Results from the (CMIP)-M-4 model intercomparison, *J. Cli.*, *19*,
1029 3337-3353.

1030 Friis, K., A. Körtzinger, J. Patsch, and D. W. R. Wallace (2004), On the temporal increase of
1031 anthropogenic CO_2 in the subpolar North Atlantic, *Deep-Sea Res. I*, *52*, 681-698.

1032

1033 Garzoli, S., O. Boebel, H. Bryden, R. A. Fine, M. Fukasawa, S. Gladyshev, G. Johnson, M.
1034 Johnson, A. MacDonald, C. S. Meinen, H. Mercier, A. Orsi, A. Piola, S. Rintoul, S. Speich,
1035 M. Visbeck, and R. Wanninkhof (2010), Progressing towards global sustained deep ocean
1036 observations, in *OceanObs'09: Sustained Ocean Observations and Information for Society*,
1037 edited by J. Hall et al., ESA Publication WPP-306.

1038 Gouretski, V. V., and K. Jancke (2001), Systematic errors as the cause for an apparent deep
1039 water property variability: Global analysis of the WOCE and historical hydrographic data,
1040 *Prog. Oceanogr.*, *48*, 337-402.

1041 Gruber, N. (1998), Anthropogenic CO_2 in the Atlantic Ocean, *Global Biogeochem. Cycles*, *12*,
1042 165-191.

1043 Gruber, N., and J. L. Sarmiento (2002), Biogeochemical/physical interactions in elemental
1044 cycles, in *The Sea: Biological-Physical Interactions in the Oceans*, edited by A. R. Robinson
1045 et al., pp. 337-399, John Wiley and Sons.

1046 Gruber, N., J. L. Sarmiento, and T. F. Stocker (1996), An improved method for detecting
1047 anthropogenic CO_2 in the oceans, *Global Biogeochem. Cycles*, *10*, 809-837.

1048 Gruber, N., C. D. Keeling, and N. R. Bates (2002), Interannual variability in the North Atlantic
1049 ocean carbon sink, *Science*, *298*, 2374-2378.

1050 Hansell, D. A., D. Olson, F. Dentener, and L. Zamora (2007), Assessment of excess nitrate
1051 development in the subtropical North Atlantic, *Mar. Chem.*, *106*, 562-579.

1052 IOC (2009), Ship-based repeat hydrography: A strategy for a sustained global program, IOC
1053 Tech. Series 89, *IOCCP Rep. No. 17/ICPO Pub. No. 142*, UNESCO.

1054 Johnson, G. C., and S. C. Doney (2006), Recent western South Atlantic bottom water warming,
1055 *Geophys. Res. Lett.*, *33*, L14614, doi:10.1029/2006GL026769.

1056 Johnson, G. C., and N. Gruber (2007), Decadal water mass variations along 20°W in the
1057 northeastern Atlantic Ocean, *Prog. Oceanogr.*, *73*, 277-295,
1058 doi:10.1016/j.pocean.2006.03.022.

1059 Johnson, G. C., J. L. Bullister, and N. Gruber (2005), Labrador Sea Water property variations in
1060 the northeastern Atlantic Ocean, *Geophys. Res. Lett.*, *32*, L07602,
1061 doi:10.1029/2005GL022404.

1062 Joos, F., G.-K. Plattner, T. F. Stocker, O. Marchal, and A. Schmittner (1999), Global warming
1063 and marine carbon cycle feedbacks on future atmospheric CO_2, *Science*, *284*, 464-467.

1064 Kawase, M., and J. L. Sarmiento (1985), Nutrients in the Atlantic thermocline, *J. Geophys. Res.*,
1065 *90*, 8961-8979.

1066 Keeling, R., and H. E. Garcia (2002), The change in oceanic O_2 inventory associated with recent
1067 global warming, *Proc., U.S. Natl. Acad. Sci.*, *99*, 7848-7853.

1068 Keeling, C. D., H. Brix, and N. Gruber (2004), Seasonal and long-term dynamics of the upper
1069 ocean carbon cycle at Station ALOHA near Hawaii, *Global Biogeochem. Cycles*, *18*,
1070 GB4006, doi:10.1029/2004GB002227.

1071 Key, R. M., A. Kozyr, C. L. Sabine, K. Lee, R. Wanninkhof, J. L. Bullister, R. A. Feely, F. J.
1072 Millero, C. Mordy, and T. H. Peng (2004), A global ocean carbon climatology: Results from
1073 Global Data Analysis Project (GLODAP), *Global Biogeochem. Cycles*, *18*, GB4031,
1074 doi:10.1029/2004GB002247.

1075 Key, R. M., T. Tanhua, A. Olsen, M. Hoppema, S. Jutterström, C. Schirnick, S. van Heuven, A.
1076 Kozyr, X. Lin, A. Velo, D. W. R. Wallace, and L. Mintrop (2010), The CARINA data
1077 synthesis project: Introduction and overview, *Earth Syst. Sci. Data*, *2*, 105-121,
1078 doi:10.5194/essd-2-105-2010.

1079 Khatiwala, S., F. Primeau, and T. Hall (2009), Reconstruction of the history of anthropogenic
1080 CO_2 concentrations in the ocean, *Nature*, *462*, 346-349, doi:10.1038/nature08526.

1081 Körtzinger, A., M. Rhein, and L. Mintrop (1999), Anthropogenic CO_2 and CFCs in the North
1082 Atlantic Ocean-A comparison of man-made tracers, *Geophys. Res. Lett.*, *26*, 2065-2068.

1083 Lee, K., F. J. Millero, and R. Wanninkhof (1997), The carbon dioxide system in the Atlantic
1084 Ocean, *J. Geophys. Res.*, *102*, 15693-15707.

1085 Lee, K., S.-D. Choi, G.-H. Park, R. Wanninkhof, T.-H. Peng, R. M. Key, C. L. Sabine, R. A.
1086 Feely, J. L. Bullister, and F. J. Millero (2003), An updated anthropogenic CO_2 inventory in
1087 the Atlantic Ocean, *Global Biogeochem. Cycles*, *17*, 1116, doi:10.1029/2003GB002067.

1088 Levine, N. M., S. C. Doney, R. Wanninkhof, K. Lindsay, and I. Y. Fung (2008), The impact of
1089 ocean carbon system variability on the detection of temporal increases in anthropogenic CO_2,
1090 *J. Geophys. Res.*, *113*, C03019, doi:10.1029/2007JC004153.

1091 Le Quéré, C., C. Röedenbeck, E. T. Buitenhuis, T. J. Conway, R. Langenfelds, A. Gomez, C.
1092 Labuschagne, M. Ramonet, T. Nakazawa, N. Metzl, and N. Gillett (2007), Saturation of the
1093 Southern Ocean CO_2 sink due to recent climate change, *Science*, *316*, 1735-1738,
1094 doi:10.1126/science.1136188.

1095 Le Quéré, C., M. R. Raupach, J. G. Canadell, G. Marland, L. Bopp, P. Ciais, T. J. Conway, S. C.
1096 Doney, R. A. Feely, P. Foster, P. Friedlingstein, K. Gurney, R. A. Houghton, J. I. House, C.
1097 Huntingford, P. E. Levy, M. R. Lomas, J. Majkut, N. Metzl, J. P. Ometto, G. P. Peters, I. C.
1098 Prentice, J. T. Randerson, S. W. Running, J. L. Sarmiento, U. Schuster, S. Sitch, T.
1099 Takahashi, N. Viovy, G. R. v. d. Werf, and F. I. Woodward (2009), Trends in the sources and
1100 sinks of carbon dioxide, *Nat. Geosci.*, *2*, 831-836, doi:10.1038/ngeo689.

1101

1102 Li, Y.-H., and T.-H. Peng (2002), Latitudinal change of remineralization ratios in the ocean and
1103 its implication for nutrient cycles, *Global Biogeochem. Cycles*, *16*, 1130,
1104 doi:10.1029/2001GB001828.

Lo Monaco, C., N. Metzl, A. Poisson, C. Brunet, and B. Schauer (2005), Anthropogenic CO_2 in the Southern Ocean: Distribution and inventory at the Indian-Atlantic boundary (World Ocean Circulation Experiment line I6), *J. Geophys. Res.*, *110*, C06010, doi:10.1029/2004JC002643.

Lovenduski, N. S., N. Gruber, S. C. Doney, and I. D. Lima (2007), Enhanced CO_2 outgassing in the Southern Ocean from a positive phase of the Southern Annular Mode, *Global Biogeochem. Cycles*, *21*, GB2026, doi:10.1029/2006GB002900.

Lovenduski, N. S., N. Gruber, and S.C. Doney (2008), Toward a mechanistic understanding of the decadal trends in the Southern Ocean carbon sink, *Global Biogeochem. Cycles*, *22*, GB3016, doi:10.1029/2007GB003139.

Marengo, J. A., C. A. Nobre, J. Tomasella, M. D. Oyama, G. S. De Oliveira, R. De Oliveira, H. Camargo, L. M. Alves, and I. F. Brown (2008), The drought of Amazonia in 2005, *J. Cli.*, *21*, 495-516.

Matear, R. J., T. A. Hirst, and B. I. McNeil (2000), Changes in dissolved oxygen in the Southern Ocean with climate change, *Geochem., Geophys., Geosyst.*, 1, 1050, doi:10.1029/2000GC000086.

Matsumoto, K., and N. Gruber (2005), How accurate is the estimation of anthropogenic carbon in the ocean? An evaluation of the ΔC^* method, *Global Biogeochem. Cycles*, *19*, GB3014, doi:10.1029/2004GB002397.

McNeil, B. I., R. J. Matear, R. M. Key, J. L. Bullister, and J. L. Sarmiento (2002), Anthropogenic CO_2 uptake by the ocean using the global chlorofluorocarbon dataset, *Science*, *299*, 235-239.

Mikaloff Fletcher, S. E., N. Gruber, A. R. Jacobson, S. C. Doney, S. Dutkiewicz, M. Gerber, M. Follows, F. Joos, K. Lindsay, D. Menemenlis, A. Mouchet, S. A. Muller, and J. L. Sarmiento (2006), Inverse estimates of anthropogenic CO_2 uptake, transport, and storage by the ocean, *Global Biogeochem. Cycles*, *20*, GB2002, doi:10.1029/2005GB002530.

Murata, A., Y. Kumamoto, K. Sasaki, S. Watanabe, and M. Fukasawa (2008), Decadal increases of anthropogenic CO_2 in the subtropical South Atlantic Ocean along 30°S, *J. Geophys. Res.*, *113*, C06007, doi:10.1029/2007JC004424.

Peng, T.-H., and R. Wanninkhof (2010), Increase of anthropogenic CO_2 in the Atlantic Ocean in last the two decades, *Deep-Sea Res. I*, *57*, 755-770, doi:10.1016/j.dsr.2010.03.008.

Peng, T.-H., R. Wanninkhof, and R. A. Feely (2003), Increase of anthropogenic CO_2 in the Pacific Ocean over the last two decades, *Deep Sea Res. II*, *50*, 3065-3082.

Pérez, F. F., M. Vázquez-Rodríguez, E. Louarn, X. A. Padín, H. Mercier, and A. F. Ríos (2008), Temporal variability of the anthropogenic CO_2 storage in the Irminger Sea, *Biogeosci.*, *5*, 1669-1679, doi:10.5194/bg-5-1669-2008.

Plattner, G.-K., R. Knutti, F. Joos, T. F. Stocker, W. v. Bloh, V. Brovkin, D. Cameron, E. Driesschaert, S. Dutkiewicz, M. Eby, N. R. Edwards, T. Fichefet, J. C. Hargreaves, C. D. Jones, M. F. Loutre, H. D. Matthews, A. Mouchet, S. A. Müller, S. Nawrath, A. Price, A. Sokolov, K. M. Strassmann, and A. J. Weaver (2008), Long-term climate commitments projected with climate carbon cycle models, *J. Cli.*, *21*, 2721-2751.

Quay, P., R. Sonnerup, J. Stutsman, J. Maurer, A. Körtzinger, X. A. Padin, and C. Robinson (2007), Anthropogenic CO_2 accumulation rates in the North Atlantic Ocean from changes in the C-13/C-12 of dissolved inorganic carbon, *Global Biogeochem. Cycles*, *21*, GB1009, doi:10.1029/2006GB002761.

Rodgers, K. B., R. M. Key, A. Gnanadesikan, J. L. Sarmiento, O. Aumont, L. Bopp, A. Ishida, M. Ishii, C. Lo Monaco, E. Maier-Reimer, N. Metzl, F. F. Pérez, R. Wanninkhof, P. Wetzel, C. D. Winn, and Y. Yamanaka (2009), Using altimetry to help explain patchy changes in hydrographic carbon measurements, *J. Geophys. Res.*, *114*, C09013, doi:10.1029/2008JC005183.

Sabine, C. L., R. A. Feely, N. Gruber, R. Key, K. Lee, J. L. Bullister, R. Wanninkhof, C. S. Wong, D. W. R. Wallace, B. Tilbrook, F. J. Millero, T.-H. Peng, A. Kozyr, T. Ono, and A. F. Rios (2004), The oceanic sink for anthropogenic CO_2, *Science*, *305*, 367-371.

Sabine, C. L., R. A. Feely, F. J. Millero, A. G. Dickson, C. Langdon, S. Mecking, and D. Greeley (2008), Decadal changes in Pacific carbon, *J. Geophys. Res.*, *113*, C07021, doi:10.1029/2007JC004577.

Sarmiento, J. L., and C. Le Quéré (1996), Oceanic carbon dioxide uptake in a model of century-scale global warming, *Science*, *274*, 1346-1350.

Sarmiento, J. L., and N. Gruber (2002), Sinks for anthropogenic carbon, *Physics Today*, *55* (8), 30-36.

Sarmiento, J. L., J. C. Orr, and U. Siegenthaler (1992), A perturbation simulation of CO_2 uptake in an ocean general circulation model, *J. Geophys. Res.*, *97*, 3621-3645.

Sarmiento, J. L., N. Gruber, M. Brzezinski, and J. Dunne (2004), High latitude controls of thermocline nutrients and low latitude biological productivity, *Nature*, *426*, 56-60.

Sarmiento, J. L., J. Simeon, A. Gnanadesikan, N. Gruber, R. M. Key, and R. Schlitzer (2007), Deep-ocean biogeochemistry of silicic acid and nitrate, *Global Biogeochem. Cycles*, *21*, GB1S90, doi:10.1029/2006GB002720.

Shulenberger, E., and L. Reid (1981), The Pacific shallow oxygen maximum, deep chlorophyll maximum, and primary production, reconsidered, *Deep-Sea Res.*, *28*, 901-919.

Solomon, S., D. Qin, M. Manning, R. B. Alley, T. Berntsen, N. L. Bindoff, Z. Chen, A. Chidthaisong, J. M. Gregory, G. C. Hegerl, M. Heimann, B. Hewitson, B. J. Hoskins, F. Joos, J. Jouzel, V. Kattsov, U. Lohmann, T. Matsuno, M. Molina, N. Nicholls, J. Overpeck, G. Raga, V. Ramaswamy, J. Ren, M. Rusticucci, R. Somerville, T. F. Stocker, R. J. Stouffer,

P. Whetton, R. A. Wood and D. Wratt, (2007), Technical Summary, in *Climate Change 2007: The Physical Science Basis. Contribution of Working Group I to the Fourth Assessment Report of the Intergovernmental Panel on Climate Change*, edited by S. Solomon et al., Cambridge University Press, Cambridge, United Kingdom and New York, N.Y.

Stott, P. A., R. T. Sutton, and D. M. Smith (2008), Detection and attribution of Atlantic salinity changes, *Geophys. Res. Lett., 35*, L21702, doi:10.1029/2008GL035874.

Stramma, L., P. Brandt, J. Schafstall, F. Schott, J. Fischer, and A. Körtzinger (2008), Oxygen minimum zone in the North Atlantic south and east of the Cape Verde Islands, *J. Geophys. Res., 113*, C04014, doi:10.1029/2007JC004369.

Stramma, L., S. Schmidtko, L. A. Levin, and G. C. Johnson (2010), Ocean oxygen minima expansions and their biological impacts, *Deep-Sea Res. I, 57*, 587-595, doi:10.1016/j.dsr.2010.01.005.

Tanhua, T., A. Biastoch, A. Körtzinger, H. Lüger, C. Boning, and D. W. R. Wallace (2006), Changes of anthropogenic CO_2 and CFCs in the North Atlantic between 1981 and 2004, *Global Biogeochem. Cycles, 20*, GB4017, doi:10.1029/2006GB002695.

Tanhua, T., A. Körtzinger, K. Friis, D. W. Waugh, and D. W. R. Wallace (2007), An estimate of anthropogenic CO_2 inventory from decadal changes in oceanic carbon content, *Proc., Natl. Acad. Sci.U.S.A., 104*, 3037-3042.

Thomas, H., A. E. Friederike Prowe, I. D. Lima, S. C. Doney, R. Wanninkhof, R. J. Greatbach, U. Schuster, and A. Corbiere (2008), Changes in the North Atlantic Oscillation influence CO_2 uptake in the North Atlantic over the past 2 decades, *Global Biogeochem. Cycles, 22*, GB4027, doi:10.1029/2007GB003167.

Thorpe, S. A. (1984), The role of bubbles produced by breaking waves in super-saturating the near surface mixed layer with oxygen, *Ann. Geophys., 2*, 53-56.

Touratier, F., and C. Goyet (2004), Applying the new TrOCA approach to estimate the distribution of anthropogenic CO_2 in the Atlantic Ocean, *J. Mar. Syst., 46*, 181-197.

Tsuchiya, M., L. D. Talley, and M. S. McCartney (1992), An eastern Atlantic section from Iceland southward across the equator, *Deep-Sea Res., 39*, 1885-1917.

Tsuchiya, M., L. D. Talley, and M. S. McCartney (1994), Water-mass distributions in the western South Atlantic: A section from South Georgia Island (54°S) northward across the equator, *J. Mar. Res., 52*, 55-81.

Vazquez-Rodriguez, M., F. Touratier, C. Lo Monaco, D. W. Waugh, X. A. Padin, R. G. J. Bellerby, C. Goyet, N. Metzl, A. F. Rios, and F. F. Perez (2009), Anthropogenic carbon distributions in the Atlantic Ocean: Data-based estimates from the Arctic to the Antarctic, *Biogeosci., 6*, 439-451.

Wallace, D. W. R. (2001), Storage and transport of excess CO_2 in the oceans: The

JGOFS/WOCE global CO_2 survey, in *Ocean Circulation and Climate*, edited by G. Siedler et al., pp. 489-521, Academic Press, AIP International Geophysics Series.

Wallace, D. W. R., P. Beining, and A. Putzka (1994), Carbon-tetrachloride and chlorofluorocarbons in the South Atlantic Ocean, 19°S, *J. Geophys. Res.*, *99*, 7803-7819.

Wanninkhof, R., and K. Thoning (1993), Measurement of fugacity of CO_2 in surface water using continuous and discrete sampling methods, *Mar. Chem.*, *44*, 189-205.

Wanninkhof, R., S. Doney, T.-H. Peng, J. L. Bullister, K. Lee, and R. A. Feely (1999), Comparison of methods to determine the anthropogenic CO_2 invasion into the Atlantic Ocean, *Tellus*, *51B*, 511-530.

Wanninkhof, R., T.-H. Peng, B. Huss, C. L. Sabine, and K. Lee (2003), Comparison of inorganic carbon system parameters measured in the Atlantic Ocean from 1990 to 1998 and recommended adjustments, *Rep. ORNL/CDIAC-140*, Oak Ridge Natl. Lab., Oak Ridge, Tenn.

Wanninkhof, R., S. C. Doney, R. D. Castle, F. J. Millero, J. L. Bullister, D. A. Hansell, M. J. Warner, C. Langdon, G. C. Johnson, and C. W. Mordy (2006), Carbon dioxide, hydrographic and chemical data obtained during the R/V *Ronald H. Brown* repeat hydrography cruise in the Atlantic Ocean: CLIVAR CO_2 section A16S_2005, *Rep. RNL/CDIAC-151, NDP-087*, Oak Ridge Natl. Lab., Oak Ridge, Tenn.

Warner, M. J., and R. F. Weiss (1985), Solubilities of chlorofluorocarbons 11 and 12 in water and seawater, *Deep-Sea Res.*, *32*, 1485-1497.

Watson, A. J., U. Schuster, D. C. E. Bakker, N. R. Bates, A. Corbière, M. González-Dávila, T. Friedrich, J. Hauck, C. Heinze, T. Johannessen, A. Körtzinger, N. Metzl, J. Olafsson, A. Olsen, A. Oschlies, A. Padin, B. Pfeil, J. M.Santana-Casiano, T. Steinhoff, M.Telszewski, A. F. Rios, D. W. R. Wallace, and R.Wanninkhof (2009), Tracking the variable North Atlantic sink for atmospheric CO_2, *Science*, *326*, 1391 – 1393, doi: 1310.1126/science.1177394.

Waugh, D. W., T. M. Hall, B. I. McNeil, R. Key, and R. J. Matear (2006), Anthropogenic CO_2 in the oceans estimated using transit time distributions, *Tellus*, *58B*, 376-389.

WOCE (1994), WOCE operations manual, section 3.1: WOCE hydrographic program, 144 pp., Woods Hole, Mass.

Yool, A., A. Oschlies, A. J. G. Nurser, and N. Gruber (2010), A model-based assessment of the TrOCA approach for estimating anthropogenic carbon in the ocean, *Biogeosci.*, *7*, 723-751.

Figure Captions

Figure 1. Cruise track occupied by the cruises along the A16 hydrographic transect with waypoints and 5° intervals depicted as circles. The northern section traverses the eastern basin of the North Atlantic while the southern transect (latitudes greater than 2°S) covers the western basin of the South Atlantic. The solid line shows the approximate location of the mid-Atlantic ridge. The SAVE 6 cruise in 1989 in the South Atlantic went to 54°S compared to 60°S for the 2005 CLIVAR/CO_2 reoccupation (Table 1).

Figure 2. Composite cross-sections (latitude versus pressure (dB)) for the 2003 and 2005 A16 cruises for: (a) salinity; (b) apparent oxygen utilization (AOU in µmol kg^{-1}); (c) total dissolved inorganic carbon (DIC in µmol kg^{-1}); (d) nitrate (NO_3^- in µmol kg^{-1}); (e) silicate (SiO_2 in µmol kg^{-1}); and (f) CFC-12 age (in years). The cutoff between the northern section, occupied in 2003, and southern section in 2005 is at 2°S.

Figure 3. Spatial differences between repeat occupations of the A16 transect for the upper 2000 dB: (a) salinity; (b) apparent oxygen utilization (ΔAOU in µmol kg^{-1}); and (c) total dissolved inorganic carbon (ΔDIC in µmol kg^{-1}). For the Northern hemisphere (60°N to 2°S) the differences are the data from 2003 minus that of 1993; for the Southern hemisphere (2°S to 54°S) the cruises occupied the line in 2005 and 1989. The data are normalized to decadal (10 year) changes by dividing all values for the southern transect (2°S to 54°S) by 10/16 to correct for the longer time between re-occupations. The scale for ΔAOU is 1.45 times that of ΔDIC such that changes due to organic matter remineralization would be reflected by the same color scheme. Concentration differences near zero are blanked (see color scales).

Figure 4. Rate of change with time in deep-water biogeochemical properties along the A16 transect between 40°N and 40°S. Deep-water values are averaged over 4° latitude bins, where deep-water is defined as potential densities referenced to 4000 dB, sigma-4, greater than 45.813 kg m^{-3} corresponding with depths greater than approximately 3500 m. The error bars are the standard error for all points within the 4° interval. All changes are expressed over a decade. The differences are displayed versus latitude for: (a) $\Delta pCO_2(20)$; (b) ΔDIC (open circles) and ΔDIC_{O2} (solid squares); and (c) ΔAOU.

Figure 5. The change in anthropogenic carbon, ΔC_{anthro}, for the time interval between cruises along the A16 transect estimated by the extended multi-linear regression (eMLR) method with separate multi-linear regressions (MLRs) determined for each of 23 distinct density ranges (Table 3). The eMLR based change in anthropogenic carbon, $\Delta DIC_{eMLRdens}$, is computed utilizing S, T, AOU, NO_3^-, and SiO_2 from 2003/2005 as input parameters. The solid lines indicate potential density horizons, sigma-0 = 27.0, 27.2, and 27.4 kg m^{-3}, respectively.

Figure 6. The eMLR based change in anthropogenic carbon, $\Delta DIC_{eMLRdens}$, versus pCFC-12 determined from the CLIVAR/CO_2 cruises in 2003 and 2005 for the pressure range of 200-2500 dB. The solid circles are for samples from 60°S to 15°S; the plus symbols are those from 15°S to 15°N; and the open circles are those from 15°N to 60°N. For clarity, only 1/3 of the data points for the 60°S to 15°S and 15°N to 60°N intervals are plotted.

Figure 7. Depth, CFC-12 age, DIC, and $\Delta DIC_{eMLRdens}$ versus latitude along potential density surface, sigma-0 = 27.3 kg m^{-3} using 2003/2005 data. (a) Depth of isopycnal surface 27.3 kg m^{-3} (dashed line, right axis) and CFC-12 age (solid line, left axis); (b) DIC (solid line), and DIC determined from the MLR technique for the 27.3-27.35 kg m^{-3} interval, MLR_{dens} (dashed line); and (c) $\Delta DIC_{eMLRdens}$ normalized to a decade.

Figure 8. Vertically integrated decadal change of anthropogenic carbon (ΔC_{anthro}) summed over 10° latitude bands along the A16 transect based on the $eMLR_{dens}$ approach (grey hatched columns), compared to the column inventory of C_{anthro} (i.e., the total uptake over the Anthropocene) as determined by *Lee et al.* [2003] (white columns, right axis).

Figure A1. Estimated DIC_{anthro} distributions for the A16 transect computed from the temporal difference in DIC, ΔDIC, for the A16 transect corrected for differences in remineralization using (a) O_2 (ΔDIC_{O2} in µmol kg^{-1}); and (b) NO_3^- (ΔDIC_{NO3} in µmol kg^{-1}). For the Northern hemisphere (60°N to 2°S) the cruises took place in 1993 and 2003; for the Southern hemisphere (2°S to 54°S) the cruise occupied the line in 1989 and 2005 but values are normalized to one decade by dividing the values in the south by 10/16. The top 2000 dB are shown.

Figure A2. Estimated DIC_{anthro} distributions for the A16 transect computed from different multi-linear regression (MLR) approaches utilizing S, T, AOU, NO_3^-, and SiO_2 as input parameters. (a) MLR determined from 1989/1993 data subtracted from 2003/2005 DIC data; (b) 1989/1993 DIC data subtracted from a MLR created from 2003/2005 data; (c) MLR determined from 1989/1993 data subtracted from the MLR determined with the 2003/2005 data using S, T, AOU, NO_3^-, and SiO_2 from 2003/2005. The approach is referred to as the extended multi-linear regression (eMLR); (d) Difference in DIC for the cruises estimated by the eMLR approach (ΔDIC_{eMLR}) with separate MLRs determined for six different latitude ranges ($\Delta DIC_{eMLRsectional}$).

Figure A3. Biases in the different MLR approaches for estimating DIC distributions. (a) DIC of 2003/2005 – MLR created from 2003/2005 data; (b) DIC of 1989/1993 – MLR created from 1989/1993 data; (c) DIC of 2003/2005 – MLR_{dens} created from 2003/2005 data; (d) DIC of 1989/1993 – MLR_{dens} created from 1989/1993 data; (e) DIC of 2003/2005 – $MLR_{sectional}$ created from 2003/2005 data; and (f) DIC of 1989/1993 – $MLR_{sectional}$ created from 1989/1993 data.

Figure A4. Estimates of ΔC_{anthro} versus pCFC-12. (a) ΔDIC_{O2} versus pCFC-12; (b) ΔDIC_{eMLR} versus pCFC-12 for the depth range of 200-2500 dB. The solid circles are for samples from 60°S to 15°S; the plus symbols are those from 15°S to 15°N; and the open circles are those from 15°N to 60°N. The corresponding plot for $\Delta DIC_{eMLRdens}$ versus pCFC is shown in Figure 6. Note the different scales used for the ΔC_{anthro} in the panels.

Table 1. Cruises used in the Analysis

Cruise Name	Expo Code	Ship	Dates[a]	Extent[b]	Hydro and Bottle Data Acess
SAVE 5	318MSAVE5	*Melville*	½/89-17/2/89	32°S-54°S	http://cchdo.ucsd.edu/data_access?ExpoCode=318MSAVE5
SAVE 6/HYDROS4	318MHYDROS4	*Melville*	21/3/89-8/4/89	32°S-0°S	http://cchdo.ucsd.edu/data_access?ExpoCode=318MHYDROS4
OACES S.ATL-91	3175MB91	*Baldrige*	15/7/91-31/7/91	5°N-42°S	http://www.aoml.noaa.gov/ocd/gcc/satl91.html
OACES N.ATL-93	3175MB93	*Baldrige*	8/7/93 -30/8/93	5°S-64°N	http://www.aoml.noaa.gov/ocd/gcc/natl93.html
CLIVAR/CO_2 A16N	33RO200306	*Brown*	19/6/03- 9/8/03	64°N-6°S	http://cdiac.ornl.gov/oceans/RepeatSections/clivar_a16n.html
CLIVAR/CO_2 A16S	33RO200501	*Brown*	17/1/05-21/2/05	60°S-2°S	http://cdiac.ornl.gov/oceans/RepeatSections/clivar_a16s.html

[a]Dates are the times that ship was occupying the transect.
[b]Listed in direction of travel.

Table 2. Decadal Change in Average Deep Water (sigma-4 >45.813) Inorganic Carbon Properties[a]

Method	N. Atlantic	Eq. Atlantic	S. Atlantic	Full Section
	(> 15°N)	(15°N-15°S)	(> 15°S)	
$\Delta pCO_2(20)$ (µatm)	6.4 (4.9)	10.6 (9.2)	10.8 (5.9)	9.3 (7.5)
ΔDIC_{O2} (µmol kg^{-1})	1.2 (1.0)	0.8 (1.3)	1.9 (1.3)	1.3 (1.2)
ΔDIC (µmol kg^{-1})	-0.5 (0.8)	-0.6 (1.9)	0.5 (1.9)	-0.2 (1.5)
$\Delta DIC_{eMLR\text{-}dens}$ (µmol kg^{-1})	0 (1.3)	0.1 (1.1)	0.6 (0.5)	0.4 (1.0)

[a]All values are averages obtained from a gridded product for sigma-4 >45.813 (≈ 3500 dB). The standard deviations are given in parenthesis

Table 3. Coefficients of the eMLR along Density Surfaces ($eMLR_{dens}$): $\Delta DIC_{eMLR} = (a + bSiO2_{t2} + c\ NO3_{t2} + d\ AOU_{t2} + eS_{t2} + fT_{t2})$

Mid	Min	Max	Temp	Salt	AOU	NO_3	SiO_2	a_o	$r^{2\,(a)}$	n[a]	res.[a]
sigma theta											
25.3	25	25.45	3.326	-2.61	-0.153	1.59	-0.920	33.6	0.92	100	5.9
25.6	25.45	25.75	4.999	-11.33	0.073	-1.24	2.067	317.0	0.96	65	5.0
25.9	25.75	26.05	-0.771	-3.62	0.104	-0.66	-2.788	159.9	0.98	77	4.7
26.2	26.05	26.35	-4.731	9.22	0.334	-2.37	-2.267	-234.5	0.99	126	3.7
26.5	26.35	26.65	1.688	-5.60	-0.095	0.46	0.385	183.4	0.99	270	3.4
26.8	26.65	26.95	2.044	1.99	-0.236	2.17	-0.683	-99.3	0.99	349	4.0
27.1	26.95	27.25	-0.210	-5.55	0.072	-1.23	0.472	214.8	0.99	563	4.2
27.3	27.25	27.35	-0.644	9.60	-0.109	0.63	0.006	-331.2	0.99	173	2.8
27.4	27.35	27.45	1.185	5.84	-0.130	0.78	0.193	-218.3	0.99	190	2.3
sigma-2											
36.45	36.4	36.5	-6.336	18.23	-0.058	0.21	-0.322	-588.2	0.98	130	2.8
36.55	36.5	36.6	2.749	-7.44	-0.183	0.83	0.002	246.6	0.97	136	2.6
36.65	36.6	36.7	4.193	-10.48	-0.100	0.62	0.161	338.9	0.98	151	2.9
36.75	36.7	36.8	6.091	-31.87	0.015	-1.30	0.383	1107.1	0.99	146	2.4
36.85	36.8	36.9	1.565	-3.90	-0.123	-0.03	0.204	137.0	0.99	206	2.4
36.95	36.9	36.98	6.868	-24.99	-0.206	0.03	0.392	856.6	0.99	232	2.8
37.00	36.98	37.03	9.364	-71.16	-0.111	-0.99	0.325	2478.8	0.99	197	3.0
37.05	37.03	37.08	7.608	-95.09	-0.085	-0.10	-0.019	3312.2	0.98	298	3.3
sigma-4											
45.825	45.813	45.838	8.049	-94.39	-0.624	3.53	0.045	3252.4	0.97	86	3.7
45.85	45.838	45.863	-4.490	-63.72	0.188	-1.01	-0.273	2250.9	0.98	106	3.3
45.875	45.863	45.888	-2.377	18.77	-0.229	4.55	-0.453	-709.7	ß0.99	110	2.3
45.9	45.888	45.913	-11.646	405.51	-0.331	-3.31	1.813	-14108.8	0.98	44	3.5
45.925	45.913	45.938	16.281	31.71	-0.341	-0.63	0.773	-1132.4	0.99	28	1.8
45.95	45.938	45.963	64.693	-425.02	-1.104	0.29	0.690	14768.4	0.99	69	2.1

[a]The count (n) correlation coefficient (r^2) and residual (res.) are those determined for the respective MLRs derived from 2003/2005 data. No straightforward error statistics can be derived for the eMLR compared to the single MLR (see text; *Friis et al*. [2004]; *Tanhua et al.* [2007]; and *Levine et al.* [2008]).

Table A1. Comparison of Specific Inventories for the Atlantic Ocean along the A16 Section (64°N-54°S) in mol m^{-2} a^{-1}

Method	N. Atlantic	Eq. Atlantic	S. Atlantic	Full Section
	(> 15°N)	(15°N-15°S)	(> 15°S)	
ΔDIC	0.82	0.23	0.56	0.58
ΔDIC_{O2}	0.92	0.60	0.86	0.82
ΔDIC_{NO3}	0.59	-0.28	0.66	0.39
ΔDIC_{eMLR}	0.59	0.68	0.78	0.68
$\Delta DIC_{eMLR\text{-}sectional}$	0.69	0.17	0.96	0.65
$\Delta DIC_{eMLRdens}$	0.57	0.20	0.76	0.53
$\Delta DIC_{C\text{-}13}$[a]	0.63 ± 0.16			
ΔDIC[b]			0.71 ± 0.1	

[a]From *Quay et al.* [2007].

[b]From *Murata et al.* [2008]: From the zonal A10 cruise along 30°S, between 35°W-15°W, 1993-2003 (see their Table 3).

1363
1364
1365

1370
1371
1372
1373
1374
1375
1376

1377
1378
1379
1380
1381
1382

1383

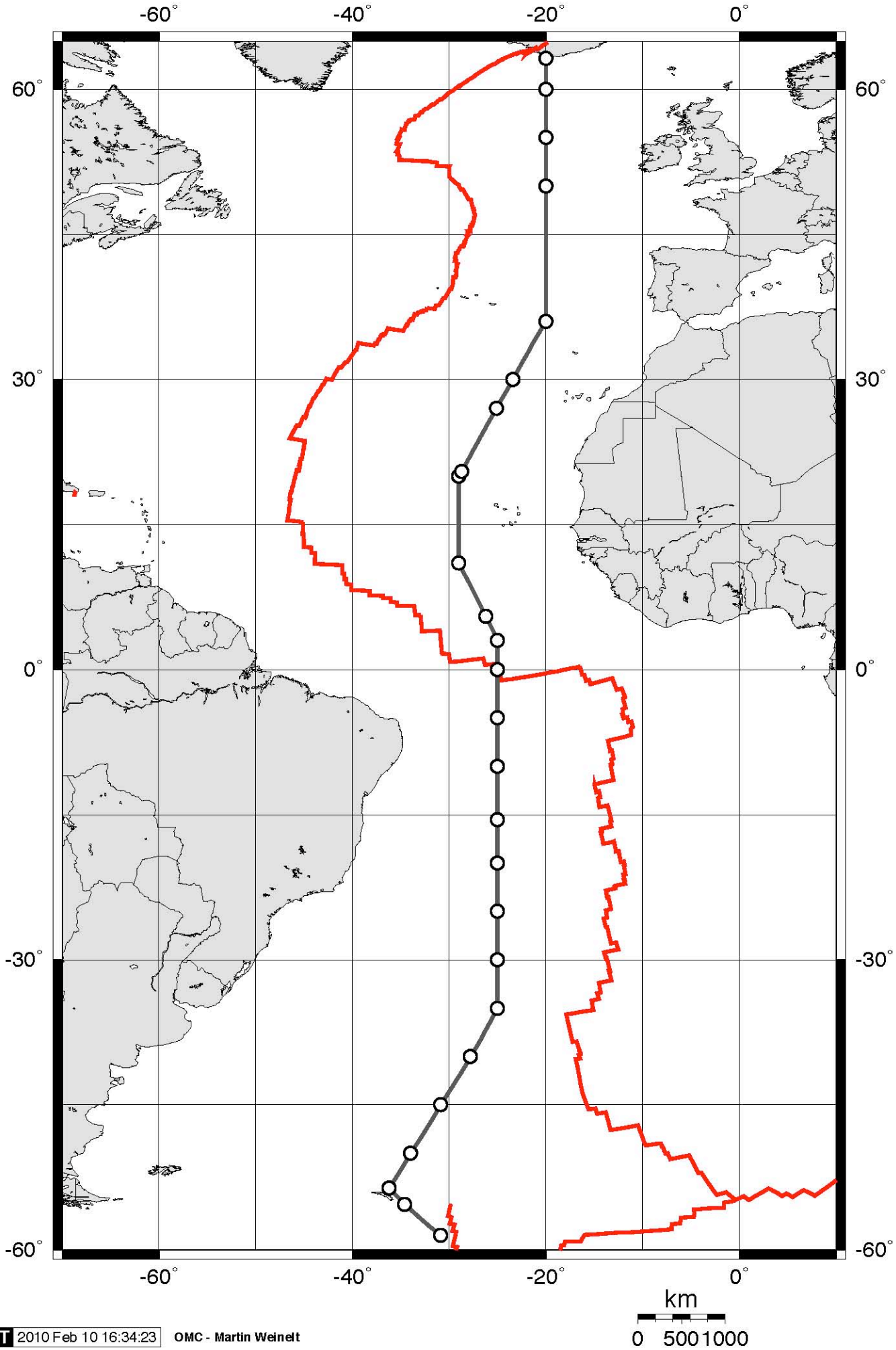
-60°
-40°
-20°
0°
60°
30°
0°
-30°
-60°
km
0 500 1000
GMT 2010 Feb 10 16:34:23
OMC - Martin Weinelt

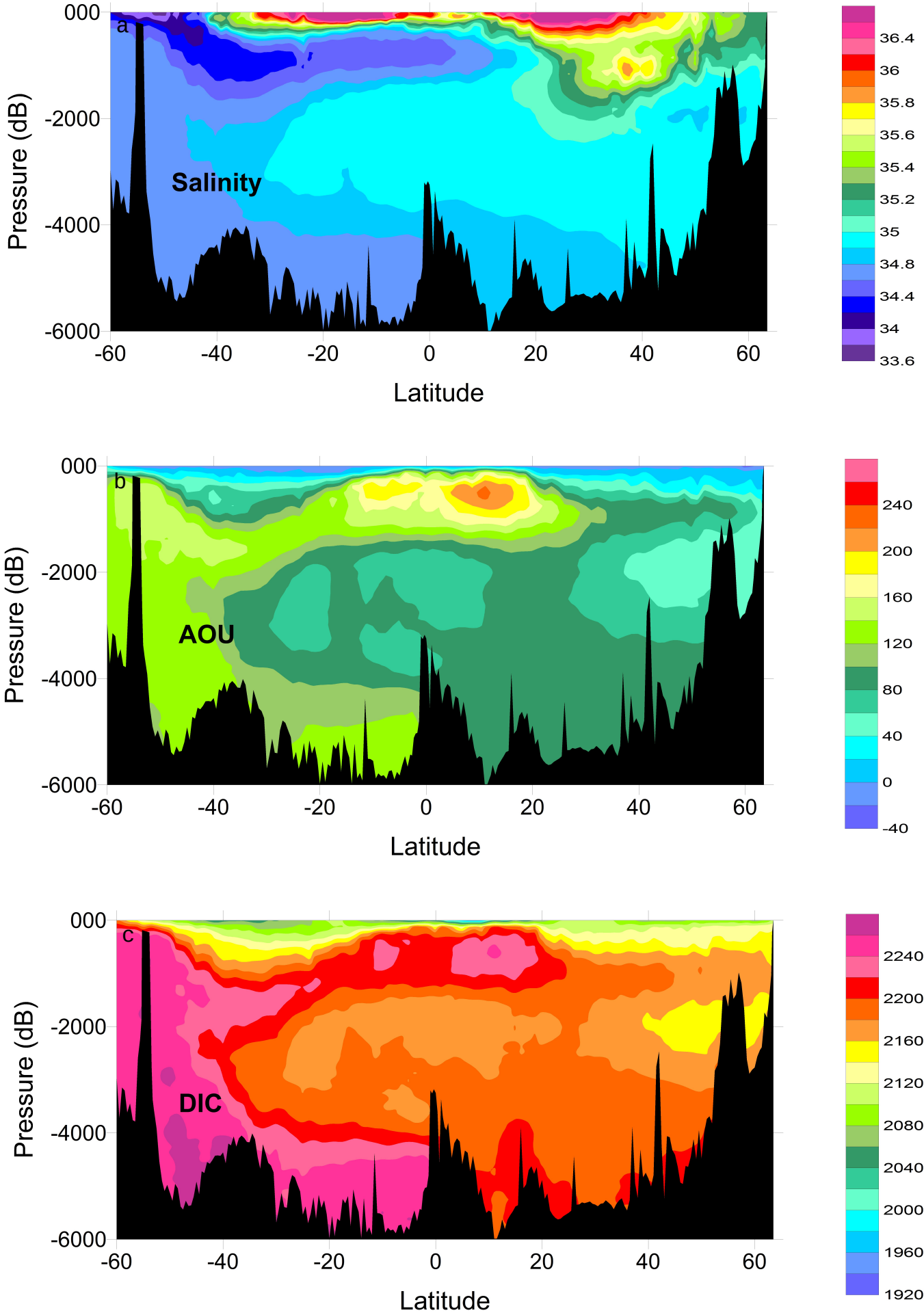
a
Salinity
Pressure (dB)
000
-2000
-4000
-6000
-60
-40
-20
0
20
40
60
Latitude
36.4
36
35.8
35.6
35.4
35.2
35
34.8
34.4
34
33.6
b
AOU
Pressure (dB)
000
-2000
-4000
-6000
-60
-40
-20
0
20
40
60
Latitude
240
200
160
120
80
40
0
-40
c
DIC
Pressure (dB)
000
-2000
-4000
-6000
-60
-40
-20
0
20
40
60
Latitude
2240
2200
2160
2120
2080
2040
2000
1960
1920

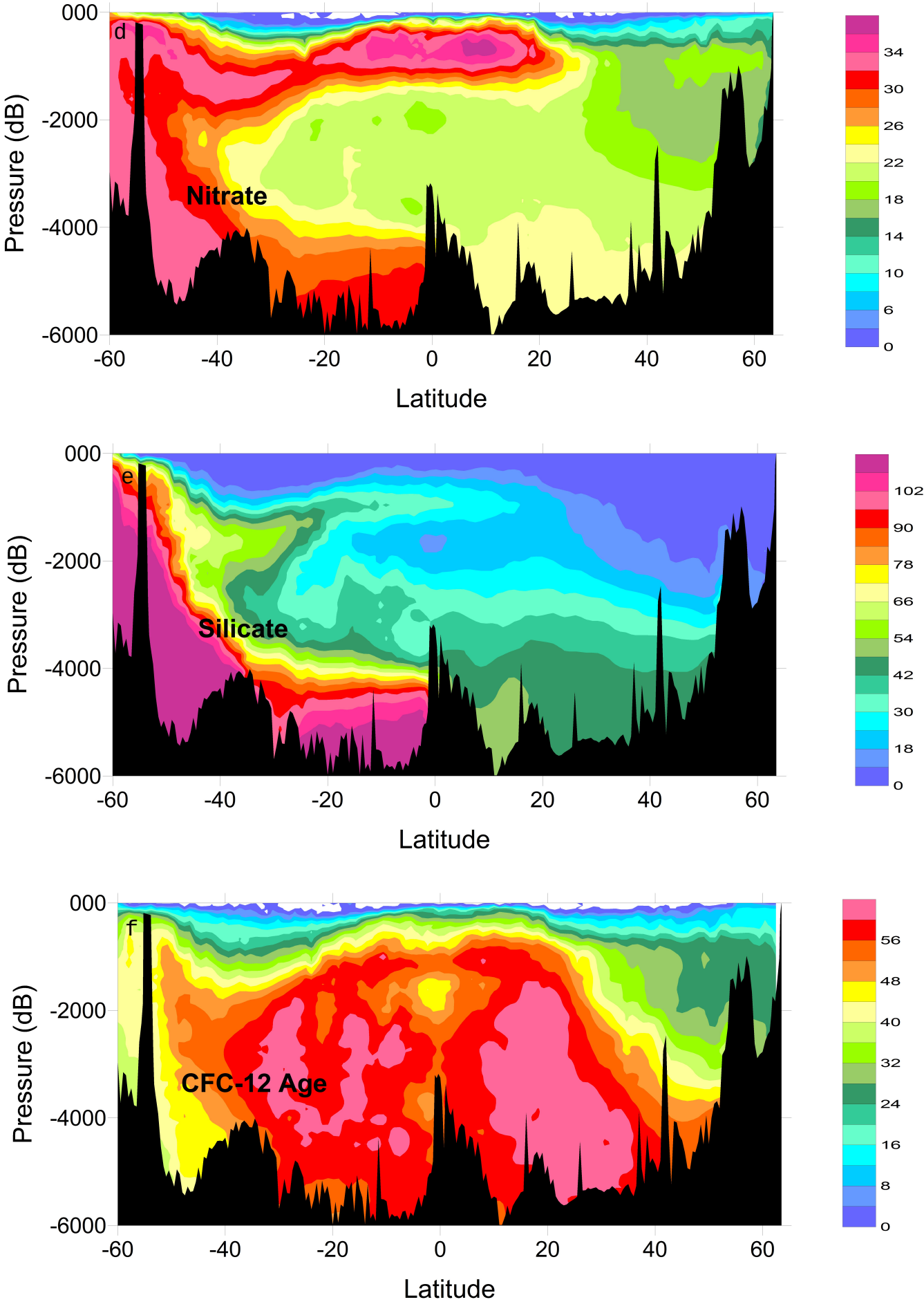
d
Nitrate
000
-2000
-4000
-6000
Pressure (dB)
-60
-40
-20
0
20
40
60
Latitude
34
30
26
22
18
14
10
6
0
e
Silicate
000
-2000
-4000
-6000
Pressure (dB)
-60
-40
-20
0
20
40
60
Latitude
102
90
78
66
54
42
30
18
0
f
CFC-12 Age
000
-2000
-4000
-6000
Pressure (dB)
-60
-40
-20
0
20
40
60
Latitude
56
48
40
32
24
16
8
0

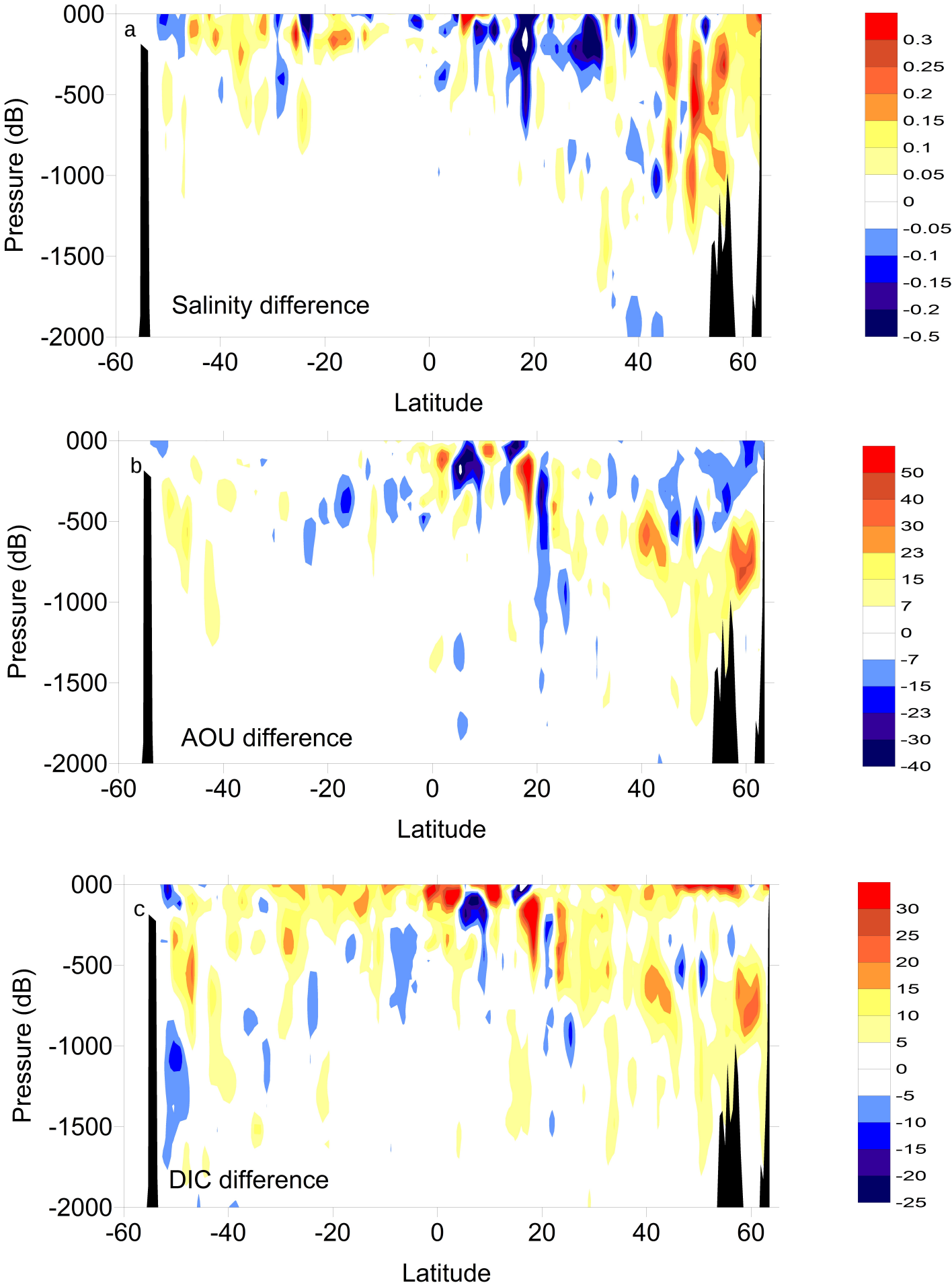
a
Salinity difference
Pressure (dB)
000
-500
-1000
-1500
-2000
-60
-40
-20
0
20
40
60
Latitude
0.3
0.25
0.2
0.15
0.1
0.05
0
-0.05
-0.1
-0.15
-0.2
-0.5
b
AOU difference
Pressure (dB)
000
-500
-1000
-1500
-2000
-60
-40
-20
0
20
40
60
Latitude
50
40
30
23
15
7
0
-7
-15
-23
-30
-40
c
DIC difference
Pressure (dB)
000
-500
-1000
-1500
-2000
-60
-40
-20
0
20
40
60
Latitude
30
25
20
15
10
5
0
-5
-10
-15
-20
-25

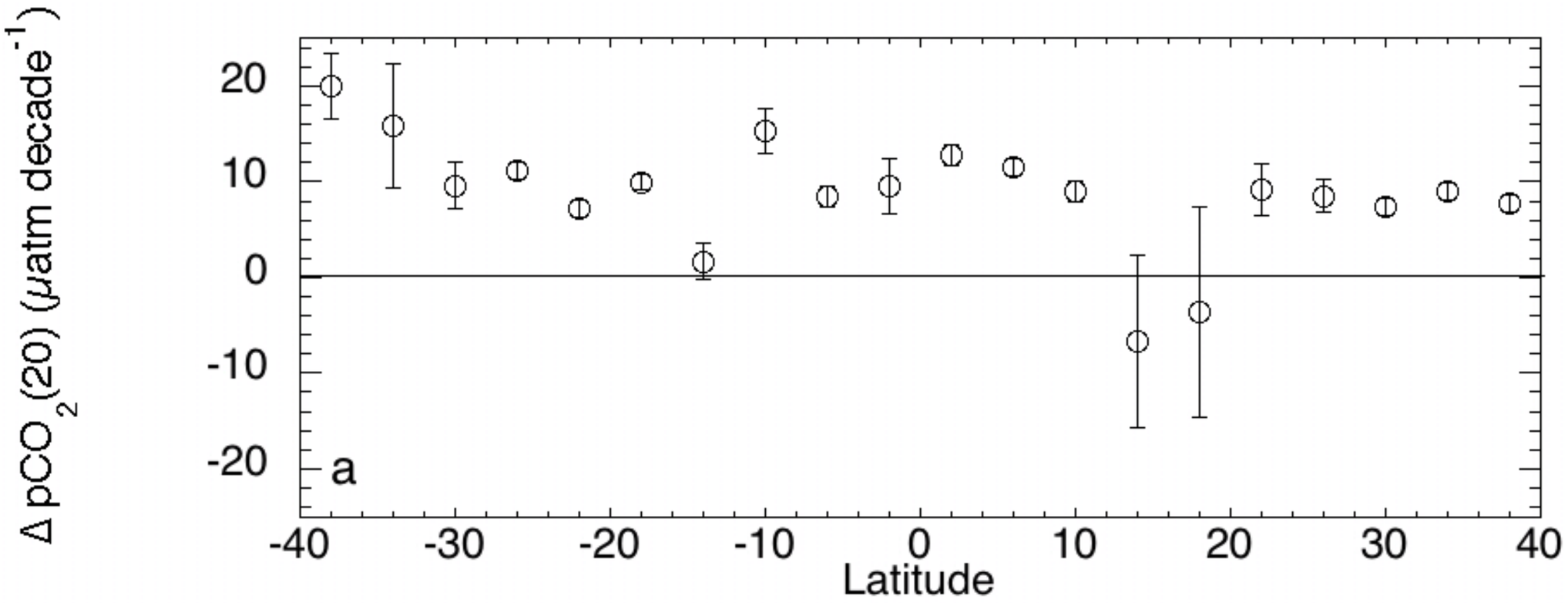
Δ pCO2(20) (μatm decade-1)
20
10
0
-10
-20
a
-40
-30
-20
-10
0
10
20
30
40
Latitude

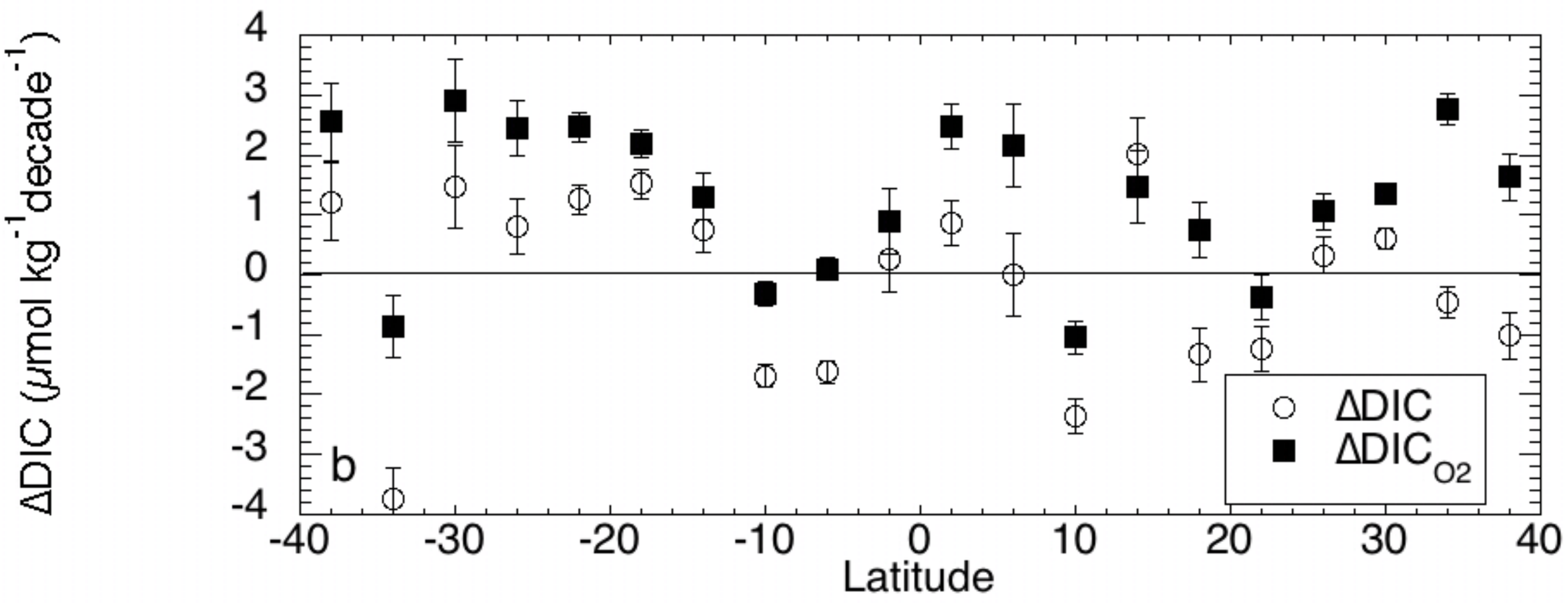
ΔDIC (μmol kg-1decade-1)
4
3
2
1
0
-1
-2
-3
-4
b
ΔDIC
ΔDIC O2
-40
-30
-20
-10
0
10
20
30
40
Latitude

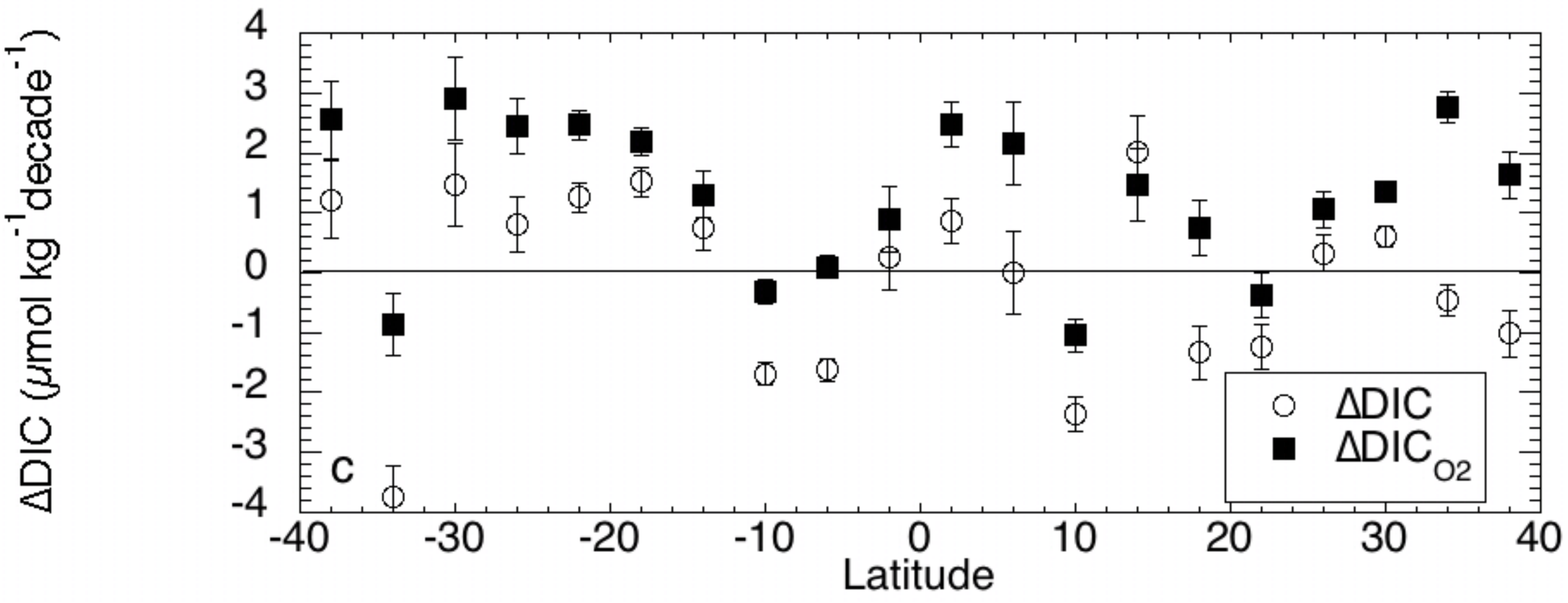
ΔDIC (μmol kg-1decade-1)
4
3
2
1
0
-1
-2
-3
-4
c
ΔDIC
ΔDIC O2
-40
-30
-20
-10
0
10
20
30
40
Latitude

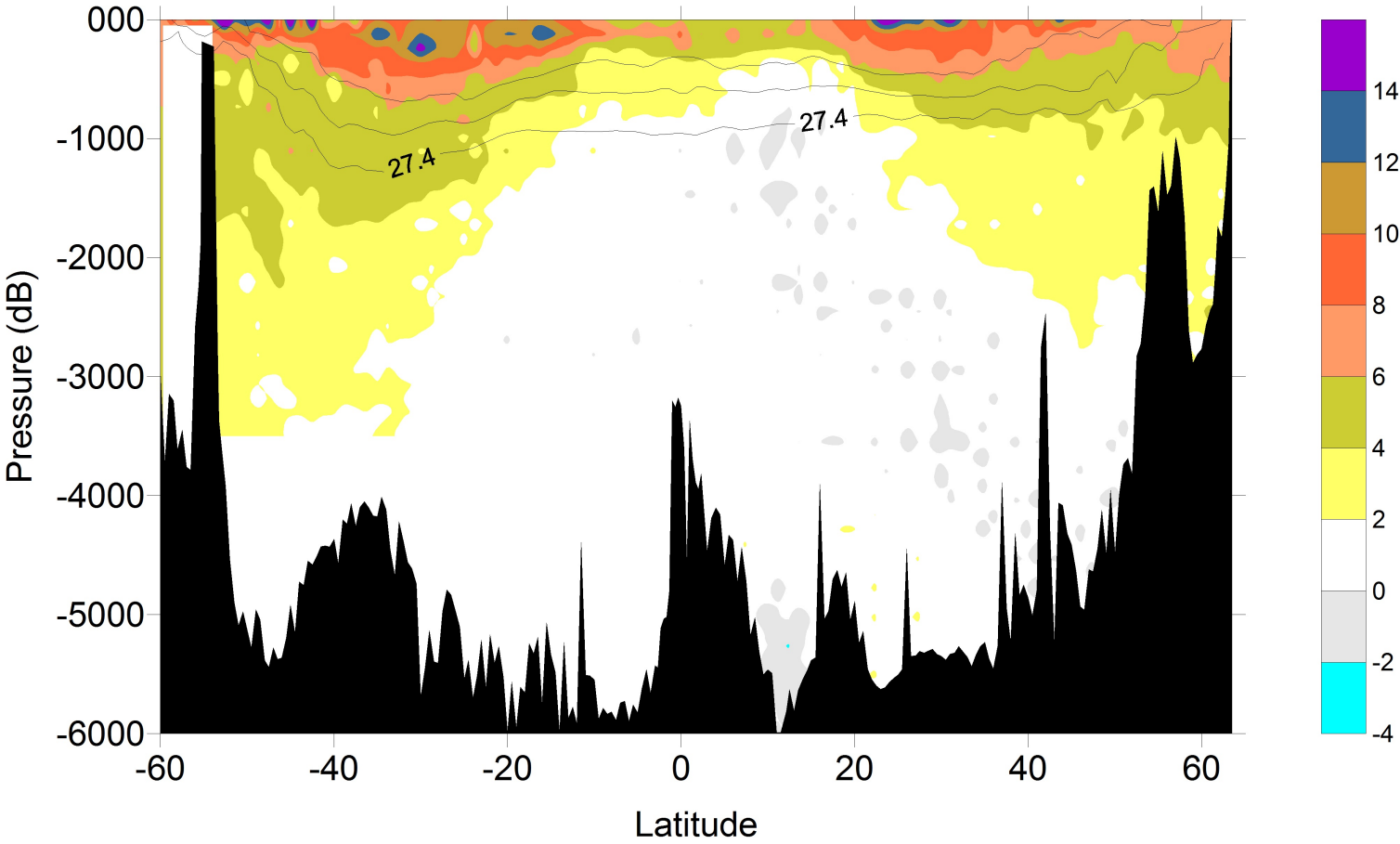
000
-1000
-2000
-3000
-4000
-5000
-6000
Pressure (dB)
-60
-40
-20
0
20
40
60
Latitude
27.4
27.4
14
12
10
8
6
4
2
0
-2
-4

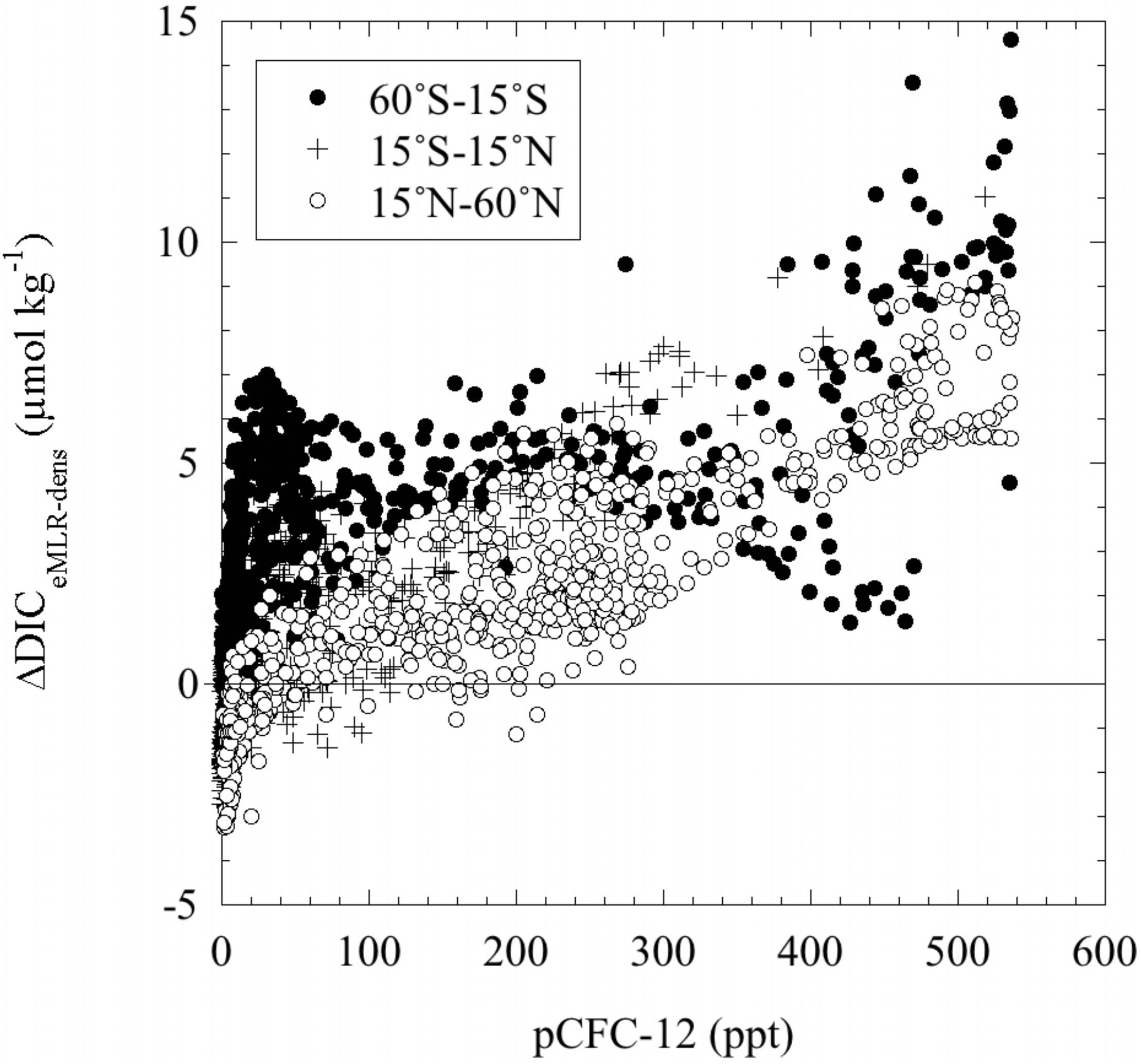
15
10
5
0
-5
0
100
200
300
400
500
600
60°S-15°S
15°S-15°N
15°N-60°N
ΔDIC eMLR-dens (μmol kg-1)
pCFC-12 (ppt)

CFC-12 age (yr)

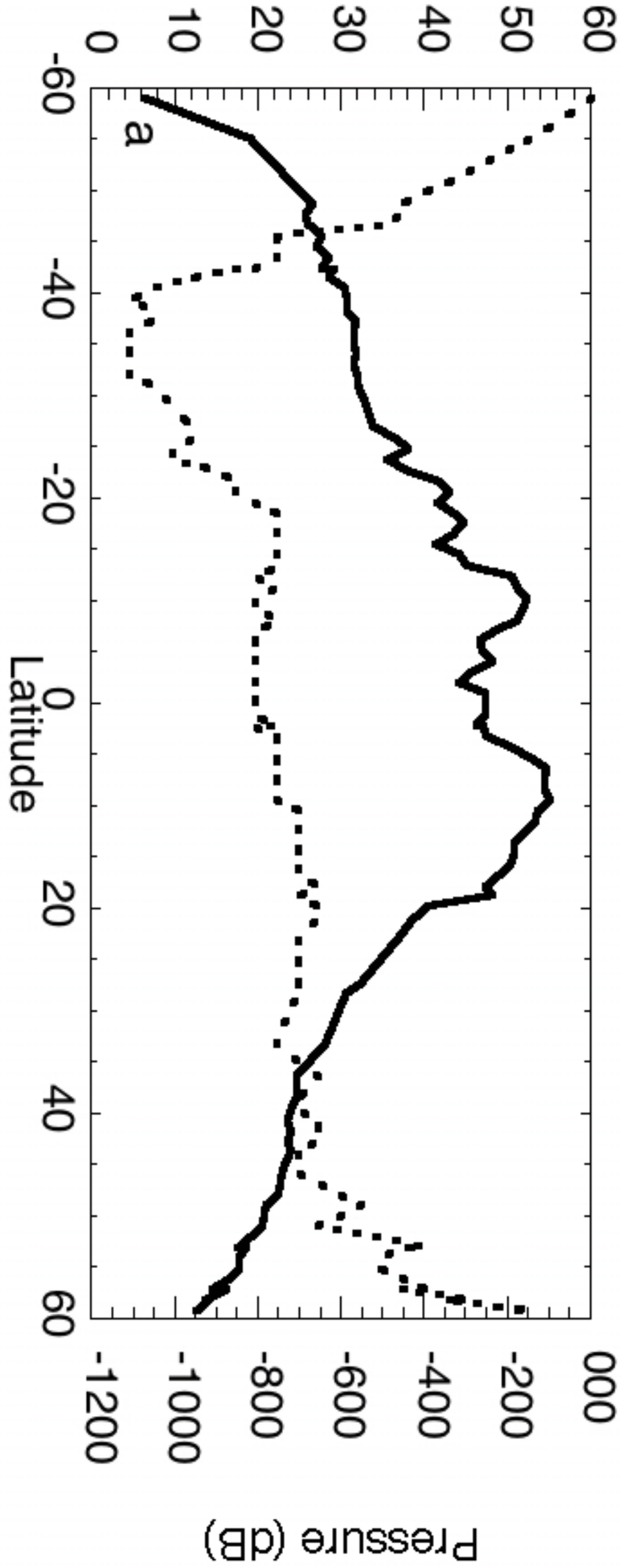

DIC (μmol kg^{-1})

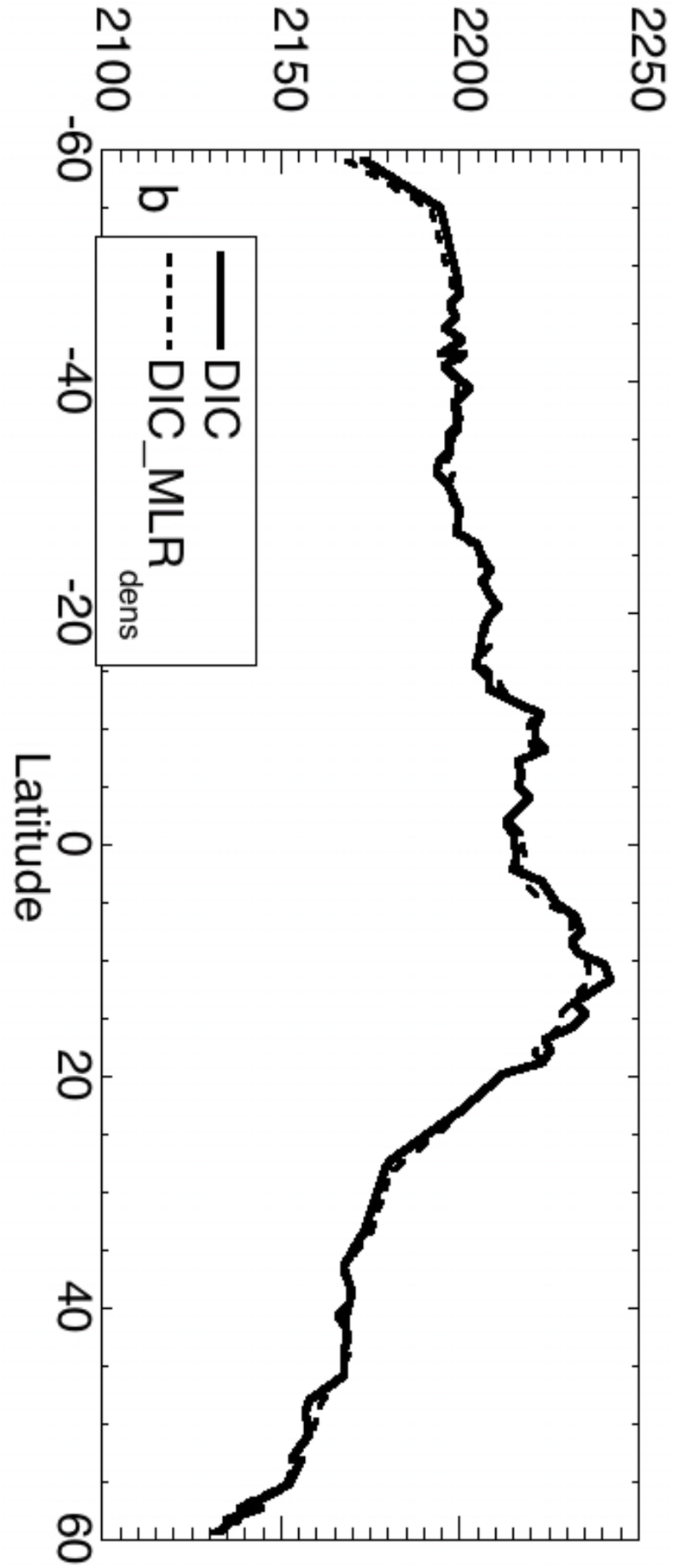

$\Delta DIC_{e\text{-}mlrdens}$ (μmol kg^{-1} decade^{-1})

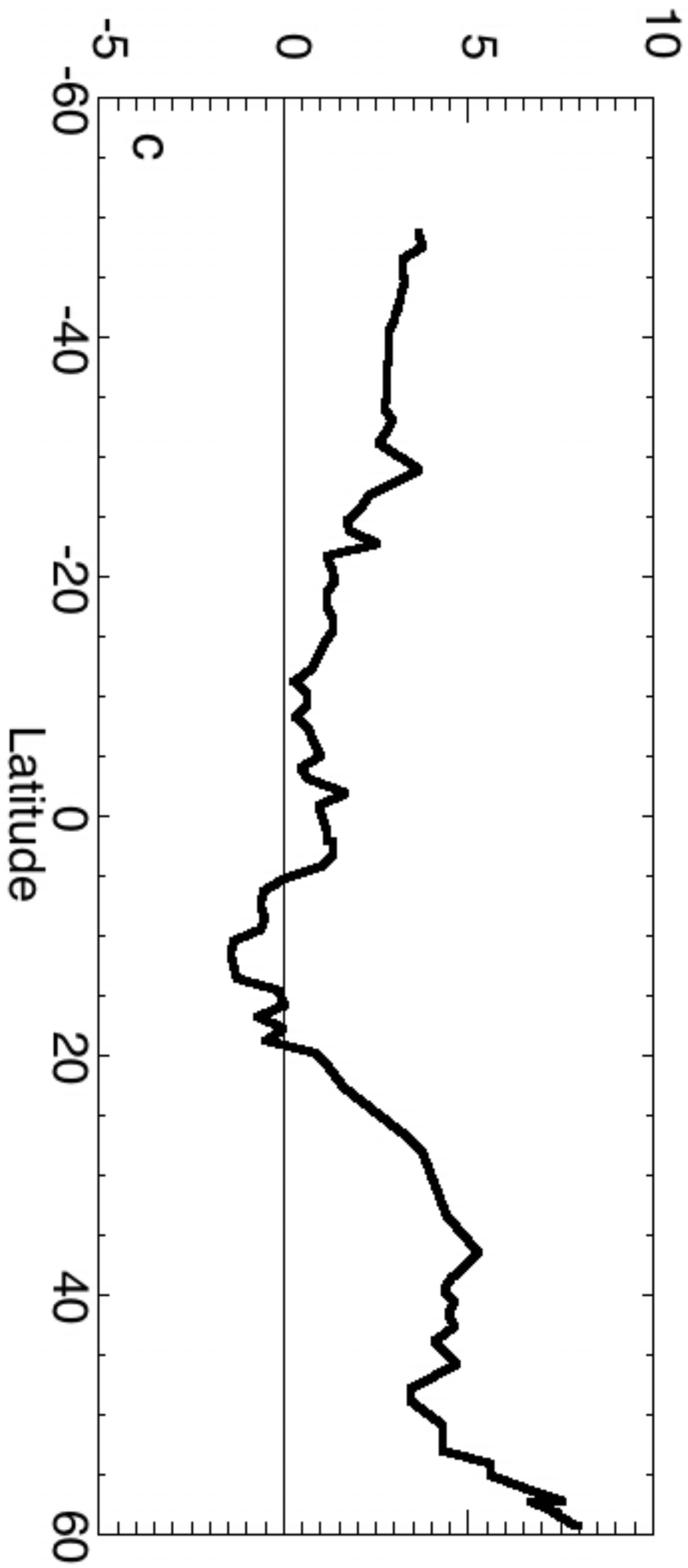

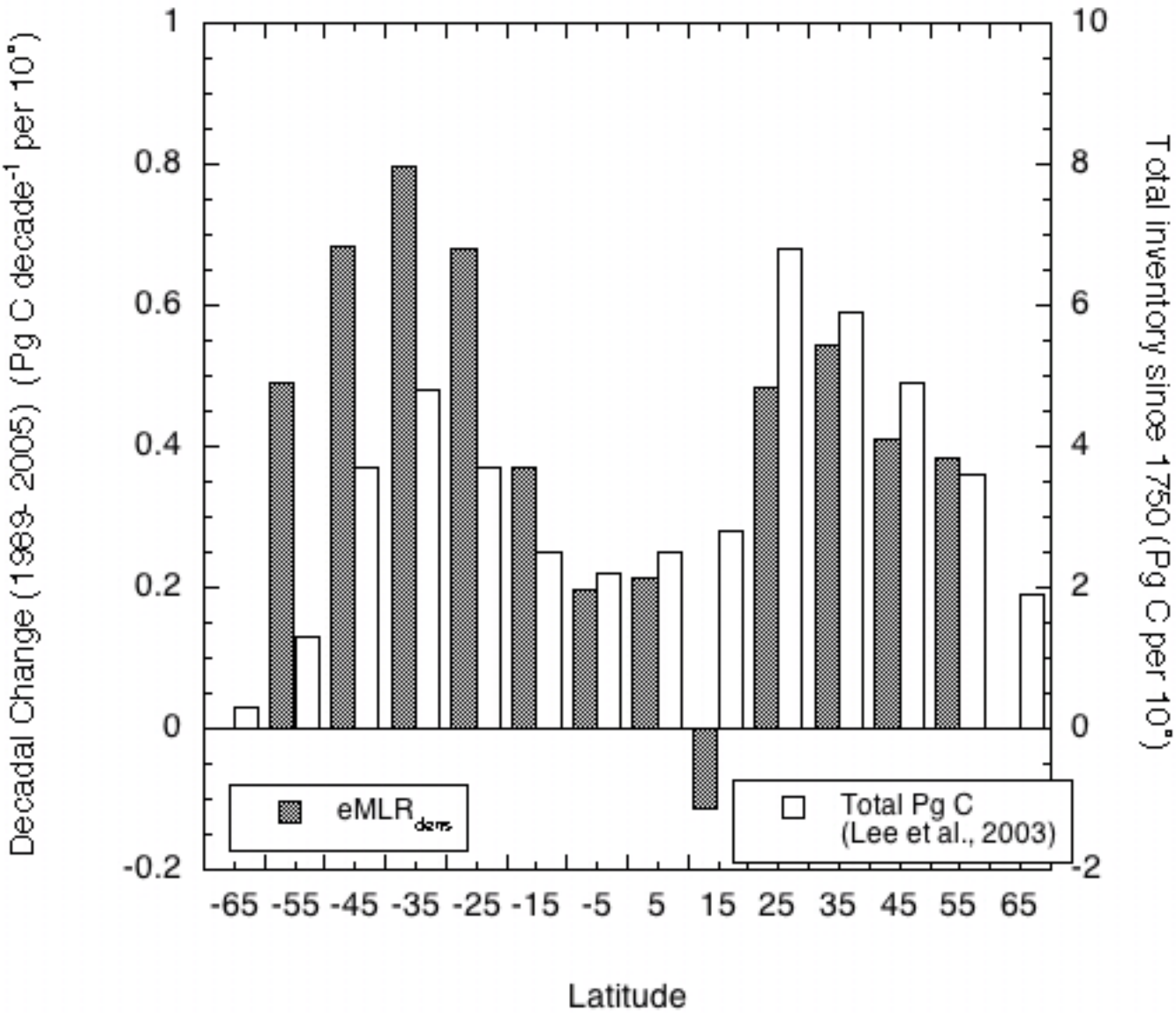
Decadal Change (1969- 2005) (Pg C decade-1 per 10°)
Total inventory since 1750 (Pg C per 10°)
Latitude
1
0.8
0.6
0.4
0.2
0
-0.2
10
8
6
4
2
0
-2
-65 -55 -45 -35 -25 -15 -5 5 15 25 35 45 55 65
eMLR
Total Pg C
(Lee et al., 2003)

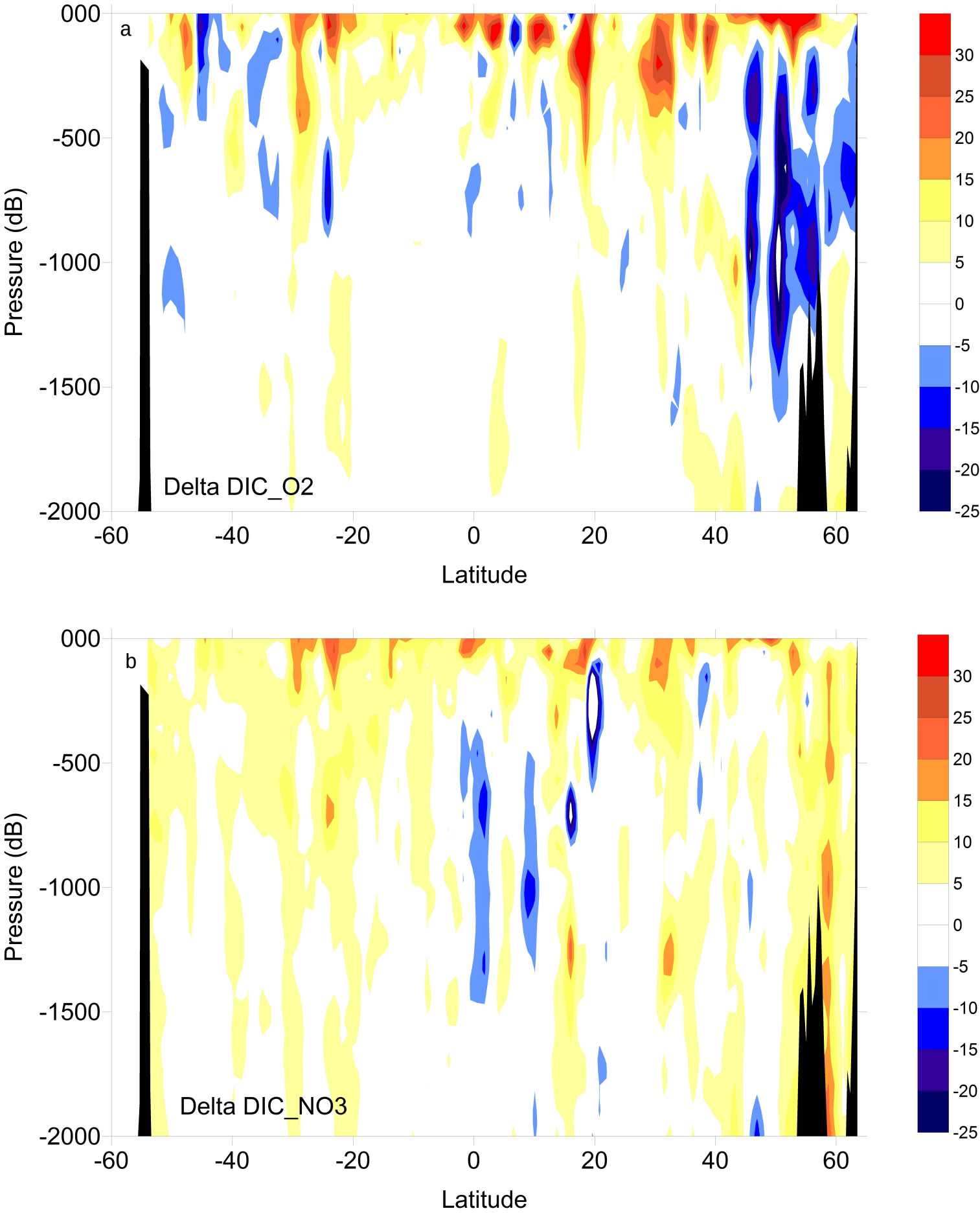
a
000
-500
-1000
-1500
-2000
Pressure (dB)
Delta DIC_O2
-60
-40
-20
0
20
40
60
Latitude
30
25
20
15
10
5
0
-5
-10
-15
-20
-25
b
000
-500
-1000
-1500
-2000
Pressure (dB)
Delta DIC_NO3
-60
-40
-20
0
20
40
60
Latitude
30
25
20
15
10
5
0
-5
-10
-15
-20
-25

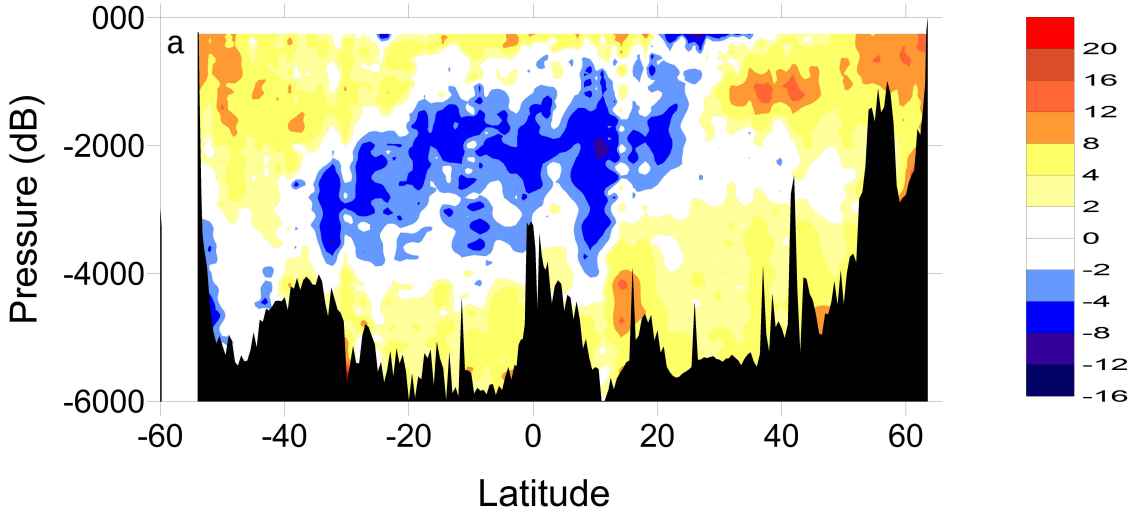
a
000
-2000
-4000
-6000
Pressure (dB)
-60
-40
-20
0
20
40
60
Latitude
20
16
12
8
4
2
0
-2
-4
-8
-12
-16

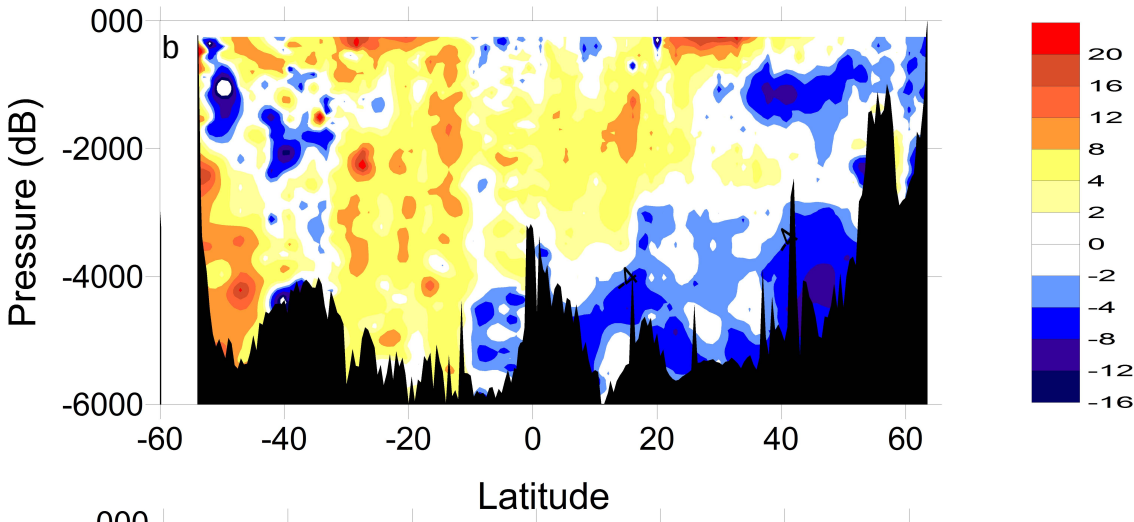
b
000
-2000
-4000
-6000
Pressure (dB)
-60
-40
-20
0
20
40
60
Latitude
20
16
12
8
4
2
0
-2
-4
-8
-12
-16

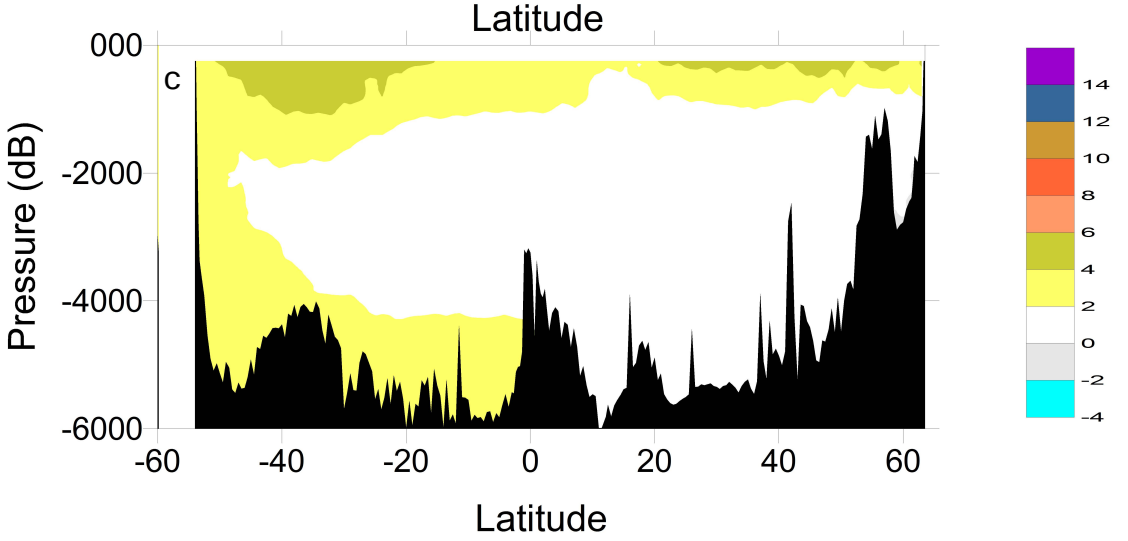
c
000
-2000
-4000
-6000
Pressure (dB)
-60
-40
-20
0
20
40
60
Latitude
14
12
10
8
6
4
2
0
-2
-4

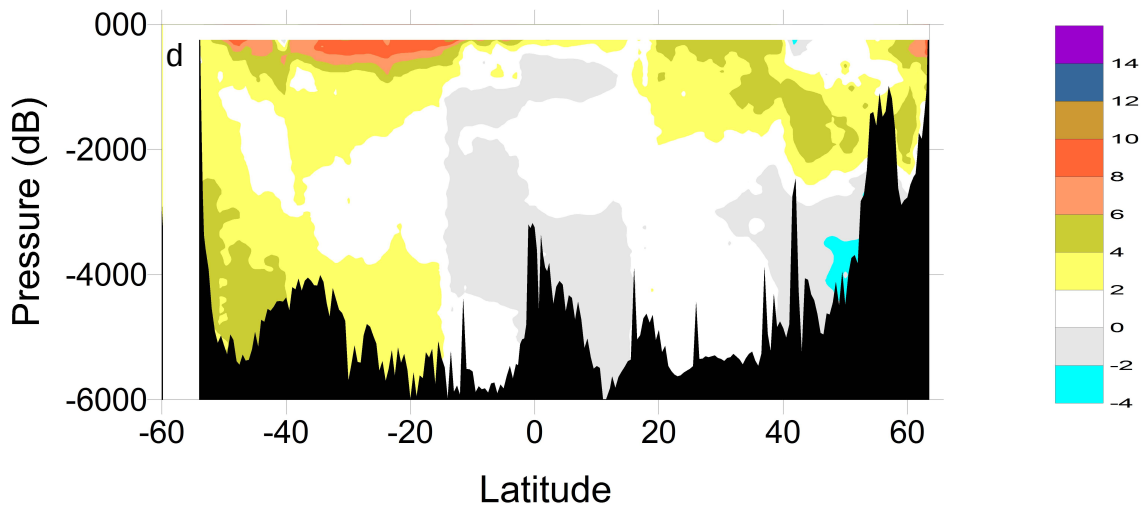
d
000
-2000
-4000
-6000
Pressure (dB)
-60
-40
-20
0
20
40
60
Latitude
14
12
10
8
6
4
2
0
-2
-4

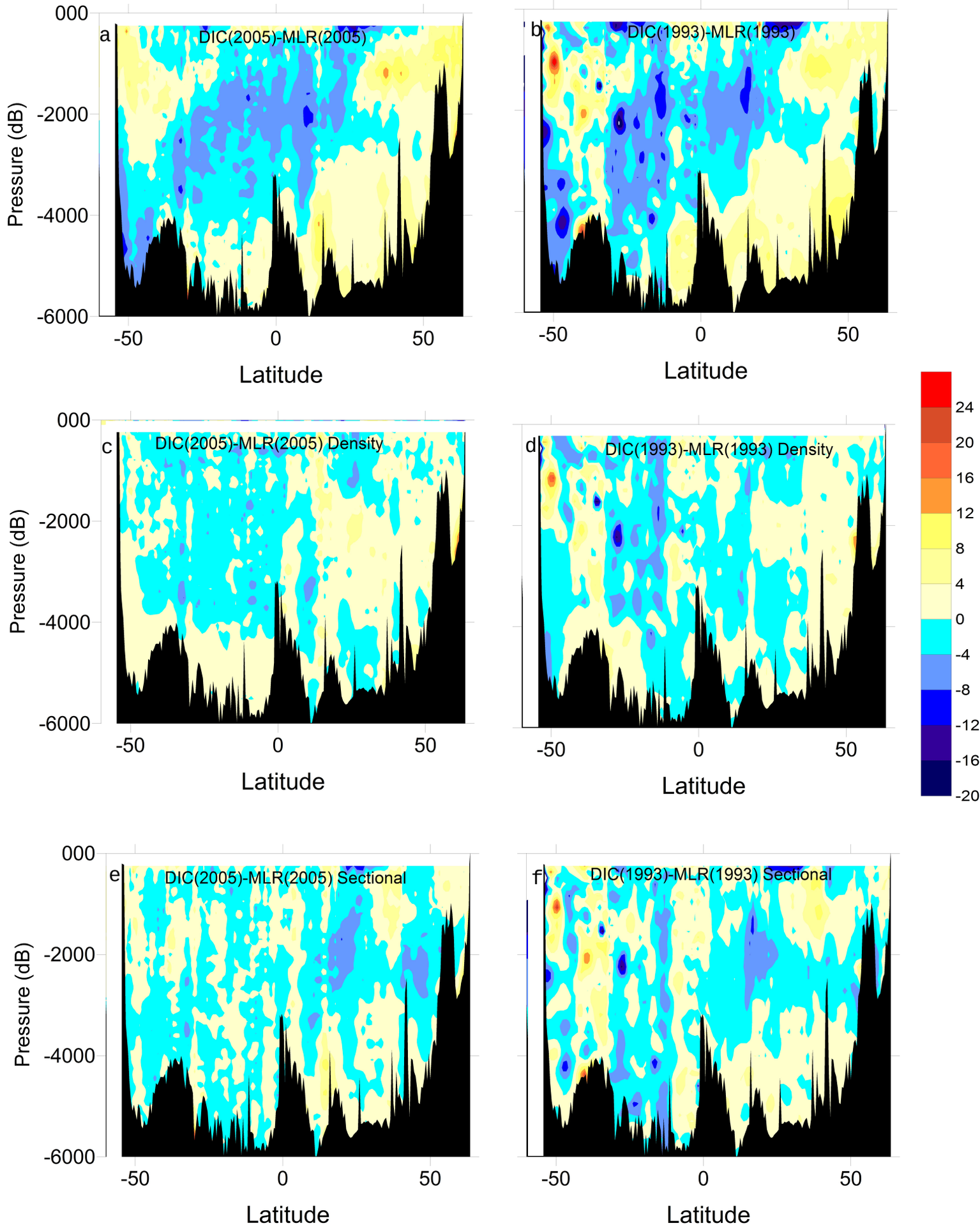
a
DIC(2005)-MLR(2005)
b
DIC(1993)-MLR(1993)
c
DIC(2005)-MLR(2005) Density
d
DIC(1993)-MLR(1993) Density
e
DIC(2005)-MLR(2005) Sectional
f
DIC(1993)-MLR(1993) Sectional
Pressure (dB)
000
-2000
-4000
-6000
-50
0
50
Latitude
24
20
16
12
8
4
0
-4
-8
-12
-16
-20

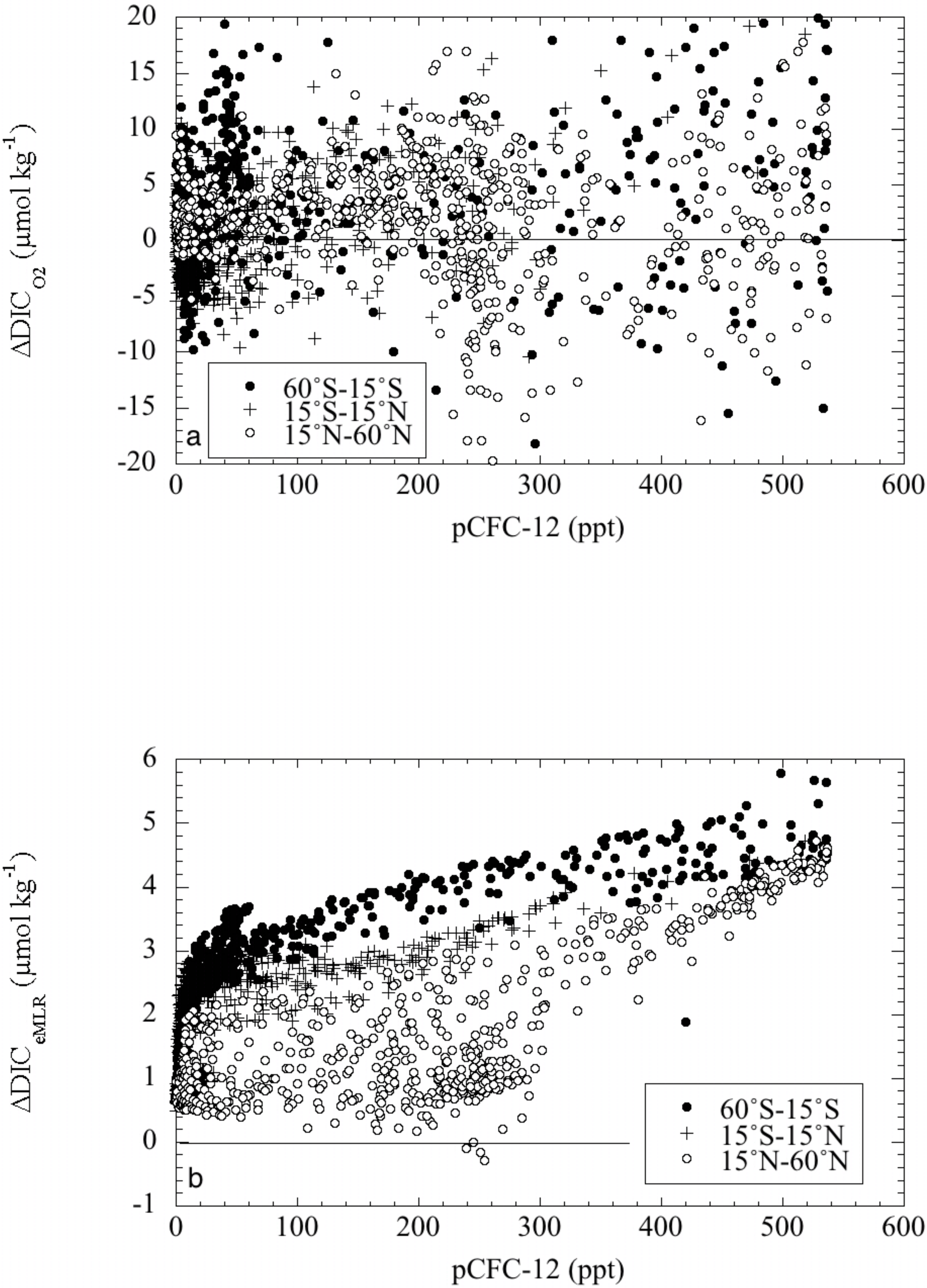
20
15
10
5
0
-5
-10
-15
-20
ΔDIC$_{O2}$ (μmol kg^{-1})
60°S-15°S
15°S-15°N
15°N-60°N
a
0
100
200
300
400
500
600
pCFC-12 (ppt)
6
5
4
3
2
1
0
-1
ΔDIC$_{eMLR}$ (μmol kg^{-1})
b
0
100
200
300
400
500
600
pCFC-12 (ppt)